

A Unified Model Spectrum for Anisotropic Stratified and Isotropic Turbulence in the Ocean and Atmosphere

ERIC KUNZE

NorthWest Research Associates, Redmond, Washington

(Manuscript received 7 May 2018, in final form 13 October 2018)

ABSTRACT

In the decade or so below the Ozmidov wavenumber $(N^3/\varepsilon)^{1/2}$, that is, on scales between those attributed to internal gravity waves and isotropic turbulence, ocean and atmosphere measurements consistently find $k^{1/3}$ horizontal wavenumber spectra for horizontal shear u_h and horizontal temperature gradient T_h and m^{-1} vertical wavenumber spectra for vertical shear u_z and strain ξ_z . Dimensional scaling is used to construct model spectra below as well as above the Ozmidov wavenumber that reproduces observed spectral slopes and levels in these two bands in both vertical and horizontal wavenumber. Aspect ratios become increasingly anisotropic below the Ozmidov wavenumber until reaching $\sim O(f/N)$, where horizontal shear $u_h \sim f$. The forward energy cascade below the Ozmidov wavenumber found in observations and numerical simulations suggests that anisotropic and isotropic turbulence are manifestations of the same nonlinear downscale energy cascade to dissipation, and that this turbulent cascade originates from anisotropic instability of finescale internal waves at horizontal wavenumbers far below the Ozmidov wavenumber. Isotropic turbulence emerges as the cascade proceeds through the Ozmidov wavenumber where shears become strong enough to overcome stratification. This contrasts with the present paradigm that geophysical isotropic turbulence arises directly from breaking internal waves. This new interpretation of the observations calls for new approaches to understand anisotropic generation of geophysical turbulence patches.


1. Introduction

This paper seeks to reproduce observed horizontal wavenumber k and vertical wavenumber m spectra in the decade or so below the Ozmidov (1965) wavenumber $k_O = (N^3/\varepsilon)^{1/2}$, that is, at scales lying between those usually attributed to isotropic turbulence and internal gravity waves (vertical wavelengths $\lambda_z \sim 1\text{--}10$ m, horizontal wavelengths $\lambda_h \sim 1\text{--}1000$ m in the ocean; $\lambda_z \sim 1\text{--}10$ km and $\lambda_h \sim 1\text{--}1000$ km in stratosphere). The Ozmidov wavenumber is the lowest wavenumber for stationary homogeneous isotropic turbulence. **Below the Ozmidov wavenumber, stratification N suppresses density overturns, diapycnal buoyancy fluxes, and isotropy,** but this does not prevent horizontal shears $u_h = ku$ from being nonlinear and turbulent ($u_h > f$). In this paper, u_h denotes the magnitude, or any component of, the horizontal shear tensor

$$\begin{pmatrix} u_x & u_y \\ v_x & v_y \end{pmatrix}$$

under a turbulence assumption of horizontal isotropy. Likewise, isotropy is assumed for horizontal wavenumber $k \sim k_x \sim k_y$. The symbol \sim denotes dependence within unknown $\sim O(1)$ scaling factors throughout this paper.

Wavenumbers several decades below the Ozmidov are thought to be dominated by internal gravity waves and geostrophic flows (Pinkel 2014; Callies et al. 2015). Vertical wavenumber spectra for internal-wave vertical shear u_z and vertical strain ξ_z are flat or weakly blue for wavenumbers below a rolloff wavenumber $m_c \sim (E_{GM}/E)[2\pi/(10\text{ m})]$ (Gargett et al. 1981; Duda and Cox 1989; Fritts et al. 1988; Gregg et al. 1993) where the rolloff wavenumber m_c is the lowest wavenumber of the m^{-1} saturated spectra, E is the nondimensional internal-wave spectral level below m_c , and $E_{GM} = 6.3 \times 10^{-5}$ its canonical value. Spectra for vertical wavenumbers $m < m_c$ are well described by the Garrett and Munk (1979) internal-wave model spectrum (Gregg and Kunze 1991).

 Denotes content that is immediately available upon publication as open access.

Corresponding author: Eric Kunze, kunze@nwra.com

Spectra above the Ozmidov and below dissipative Kolmogorov and Batchelor (1959) wavenumbers are well explained by isotropic turbulence theory (Batchelor 1953; Tennekes and Lumley 1972; Thorpe 2005). Above the Ozmidov wavenumber $m_O \sim k_O$, shear spectra rise with slope $+1/3$ before falling off sharply above the Kolmogorov (1941) wavenumber $m_K \sim k_K \sim (\varepsilon/\nu^3)^{1/4}$. Isotropic turbulence is nonlinear and lognormal. Internal waves are linked to isotropic turbulence production by weakly nonlinear internal-wave/wave interaction theory (McComas and Müller 1981; Henyey et al. 1986) such that turbulent dissipation rate $\varepsilon \propto E^2$ (Gregg and Kunze 1991; Polzin et al. 1995).

In the wavenumber band between internal waves and isotropic turbulence, that is, the decade or so below the Ozmidov wavenumber that is the focus here, motions are also nonlinear with $u_z \sim N$. In this paper, a spectral model is constructed using dimensional scaling with the turbulent energy cascade or dissipation rate ε , background buoyancy frequency N , Coriolis frequency f , and horizontal wavenumber k (Table 1). The model is guided by and seeks to replicate the following features in the ocean, atmosphere, and numerical simulations:

- 1) Spectral slopes of $+1/3$ for several decades in horizontal wavenumber k below the Ozmidov wavenumber for horizontal gradient quantities such as horizontal shear u_h and horizontal temperature gradient T_h (Fig. 1a). In the ocean, a $+1/3$ gradient spectral slope is found at horizontal wavelengths $\lambda_h \sim 1\text{--}100$ m with towed thermistors (Ewart 1976; Klymak and Moum 2007; Moum 2015) and seismic sections (Holbrook and Fer 2005; Sheen et al. 2009; Holbrook et al. 2013; Falder et al. 2016; Fortin et al. 2016). In the atmosphere, Nastrom and Gage (1985) find equivalent $-5/3$ spectral slopes for both along- and across-track horizontal velocity components and temperature at $\lambda_h \sim 5\text{--}500$ km. At lower wavenumbers, the spectrum is redder, with gradient spectral slopes of from -1 to 0 . A $+1/3$ gradient spectral slope is also found in numerical simulations of stratified turbulence (Riley and deBruynKops 2003; Waite and Bartello 2004; Lindborg 2006; Brethouwer et al. 2007). A $+1/3$ gradient spectral slope is thought to characterize a turbulent energy cascade that depends only on cascade rate ε and wavenumber k with no intermediate sources or sinks (e.g., Kolmogorov 1941). While other explanations cannot be ruled out based on spectral slope alone, a uniform forward (downscale) energy cascade in horizontal wavenumber k will be assumed here based on point 4 below.
- 2) Spectral levels that rise and fall with turbulent kinetic energy dissipation rates ε below as well as above the Ozmidov wavenumber (Fig. 1a) in T_h measurements

TABLE 1. Fundamental dimensional variables. The vertical wavenumber $m \sim k$ for isotropic turbulence $(N^2/\varepsilon)^{1/2} < k < (\varepsilon/\nu^3)^{1/4}$ and $m \sim Nk^{1/3}/\varepsilon^{1/3}$ for anisotropic stratified turbulence $(f^2/\varepsilon)^{1/2} < k < (N^2/\varepsilon)^{1/2}$.

Variable	Description	Units
ε	Cascade rate	$\text{m}^2 \text{s}^{-3}$
N	Buoyancy frequency	rad s^{-1}
f	Coriolis frequency	rad s^{-1}
ν	Kinematic molecular viscosity	$\text{m}^2 \text{s}^{-1}$
κ	Scalar molecular diffusivity	$\text{m}^2 \text{s}^{-1}$
$k = \ell_h^{-1} = 2\pi/\lambda_h$	Horizontal wavenumber	rad m^{-1}
$m = \ell_z^{-1} = 2\pi/\lambda_z$	Vertical wavenumber	rad m^{-1}

- (Klymak and Moum 2007). This indicates a quantitative dynamical connection between (i) isotropic turbulence above the Ozmidov wavenumber ($k > k_O$) and (ii) the horizontal wavenumber k spectrum below the Ozmidov wavenumber ($k < k_O$). This observation has led to a parameterization of turbulent dissipation rate ε in terms of spectral levels below the Ozmidov wavenumber in horizontal wavenumber k that is now routinely being applied to seismic measurement sections (Sheen et al. 2009; Holbrook et al. 2013; Falder et al. 2016; Fortin et al. 2016) and drifter array data (Poje et al. 2017) in the ocean.
- 3) No change in spectral slopes or levels across the Ozmidov wavenumber in horizontal wavenumber k spectra for T_h (Fig. 1a; Klymak and Moum 2007). This again indicates a smooth transition between the dynamics below the Ozmidov wavenumber and isotropic turbulence above the Ozmidov wavenumber. It also suggests no additional sources or sinks at $k = k_O$, at odds with the conventional wisdom that isotropic turbulence is generated by breaking internal waves at the Ozmidov wavenumber.
 - 4) Inference of a forward, or downscale, energy cascade below the Ozmidov wavenumber in horizontal wavenumber k transfer spectra for atmospheric scalars (Lindborg and Cho 2000), oceanic surface drifter trajectories (Poje et al. 2017), and numerical simulations (Waite and Bartello 2004; Lindborg 2006; Brethouwer et al. 2007). This, along with points 2 and 3 above, suggests that the source for geophysical turbulence ($k > k_O$) lies below the Ozmidov wavenumber ($k < k_O$). Lindborg (2005) reported that the forward energy cascade was not suppressed by rotation for $u_h > 0.1f$ (Rossby number $\delta_f = u_h/f < 0.1$, also denoted Ro). Lindborg (2006) reported that a forward cascade was associated with $(\nabla \times \mathbf{v}) \cdot \nabla b \sim (\nabla \times \mathbf{v})/N^2$, that is, buoyancy gradient anomalies comparable to the background stratification N^2 , while an inverse cascade with $(\nabla \times \mathbf{v}) \cdot \nabla b \ll (\nabla \times \mathbf{v})/N^2$, that is, buoyancy gradient anomalies weak compared to the background

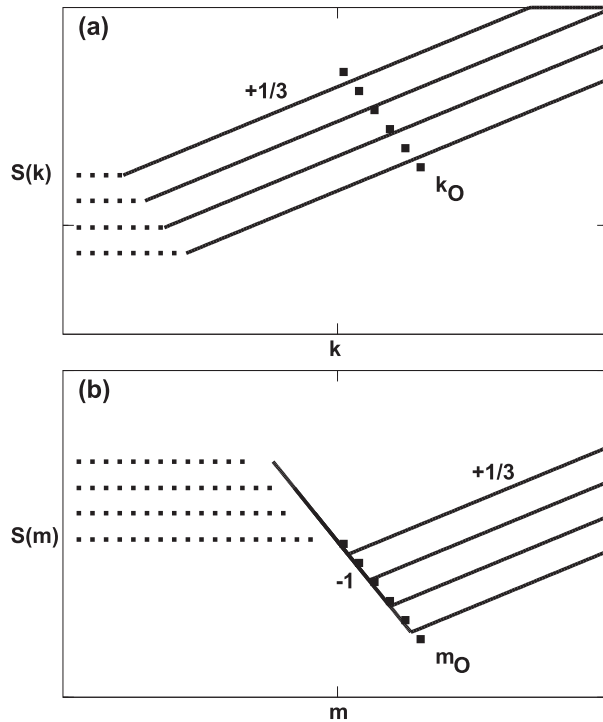


FIG. 1. Schematic interpretation of log-log spectra above and below the Ozmidov wavenumber $k_O = m_O = (N^3/\varepsilon)^{1/2}$ for gradient quantities such as (a) horizontal buoyancy gradient b_h and horizontal shear u_h in horizontal wavenumber k , and (b) vertical shear u_z or vertical buoyancy gradient b_z in vertical wavenumber m . Dotted lines at low wavenumbers correspond to weakly nonlinear internal waves or balanced motions. Spectral slopes are labeled. The thick dotted lines track $S(k_O)$ vs k_O in (a) and $S(m_O)$ vs m_O in (b). Spectra above the Ozmidov wavenumber $k_O = m_O$ describe isotropic turbulence. Spectral levels go as $\varepsilon^{2/3}$ in the isotropic band ($k = m > k_O = m_O$) and as $\varepsilon^{1/2}$ in the “internal wave” band. The -1 slope band in vertical wavenumber with invariant spectral level in (b) is referred to as the saturated spectrum.

stratification as was assumed by Charney (1971), Riley et al. (1981), and Lilly (1983). Lindborg (2006) also found that vertical nonlinearity $w\partial/\partial z$ was necessary for a forward cascade, suggesting that it needs to be included and may be comparable to horizontal nonlinear terms in the conservation equations.

- 5) Vertical wavenumber m spectra for vertical shear $u_z = \partial u/\partial z = mu$ and vertical strain $\xi_z = \partial \xi/\partial z = m\xi$ behaving as m^{-1} for the decade or so below the Ozmidov wavenumber (Fig. 1b), corresponding to vertical wavelengths $\lambda_z \sim 0.1$ – 10 m in the ocean (Gargett et al. 1981; Gregg et al. 1993) and ~ 1 – 10 km in the atmosphere (Dewan 1979; Fritts 1984; Fritts et al. 1988; Dewan and Good 1986; Smith et al. 1987). Gregg et al. (1993) reported redder finescale spectral slopes of -1.4 at low latitudes in the Pacific.

- 6) Invariant spectral levels in this m^{-1} band (Fig. 1b), for example, $S[u_z/N](m) \sim S[\xi_z](m) \sim m^{-1}$ {where $S[X](m)$ denotes the spectrum S for variable X as a function of m } for normalized vertical shear and vertical strain so that this band is referred to as the saturated spectrum (Dewan 1979; Gargett et al. 1981; Fritts 1984; Fritts et al. 1988; Dewan and Good 1986; Smith et al. 1987; Gregg et al. 1993; Dewan 1997). Its invariance contrasts with covarying internal-wave (lower m) and turbulent (higher m) spectral levels that rise and fall together (Fig. 1b).

Riley and Lindborg (2008) provide a concise review of observed submesoscale horizontal and finescale vertical wavenumber spectra in the atmosphere and ocean that are summarized here with Fig. 1.

There have been numerous explanations put forward for the level and slope of the saturated vertical wavenumber spectrum ($m_c < m < m_O$), and the corresponding horizontal wavenumber k spectrum ($k < k_O$), lying between internal-wave (lower m) and isotropic turbulence wavenumber bands:

- 1) A purely kinematic effect of vertical self-straining $\partial \xi/\partial z$ by internal gravity waves (Eckermann 1999). This might explain the m^{-1} vertical wavenumber spectrum but this one-dimensional (1D) model does not address the $k^{1/3}$ horizontal wavenumber gradient spectrum.
- 2) Breaking of upward-radiating internal waves in the stratosphere as they propagate into rarefying density and saturate in a downscale, or forward, energy cascade (Dewan 1979; Fritts 1984; Dewan and Good 1986; Smith et al. 1987; Dewan 1997). This argument does not apply in the ocean, where density varies by only a few percent, and again does not address the $k^{1/3}$ horizontal wavenumber gradient spectrum.
- 3) A transition from weak to strong internal-wave/wave interactions based on ray-tracing simulations (Hines 1993), though it was recognized that the transition to nonlinearity may no longer be wavelike.
- 4) Anisotropic stratified turbulence, sometimes referred to as blini, pancake eddies, or vortical motion (Riley et al. 1981; Lilly 1983; Müller et al. 1986, 1988). This physics has been extensively investigated numerically (Billant and Chomaz 2000, 2001; Riley and deBruynKops 2003; Waite and Bartello 2004; Lindborg 2005, 2006; Brethouwer et al. 2007; Bartello and Tobias 2013; Maffioli 2017) to uncover the underlying spectral behavior for anisotropic turbulence, as well as to explore generation (Waite and Bartello 2006a,b) and the transition to isotropic turbulence. In the ocean, Polzin et al. (2003) ascribed features in finescale u , v , and b vertical profiles and current-meter time series that were *not* consistent with linear internal gravity waves to

linear vortical motions (vortical mode or geostrophy). The subinertial energy ratio in current-meter data was used to assign an aspect ratio $k/m \sim O(f/N)$ under the assumption that this signal represented Doppler-shifted geostrophic finestructure of zero Lagrangian frequency. They argued that their inferred vortical finestructure could only arise from an upscale (inverse) cascade from irreversible mixing at the microscale, which is in the opposite direction to the transfer spectra inferences quoted earlier. A more recent study by Pinkel (2014) used profile time series to transform shear and strain profiles onto isopycnal (semi-Lagrangian SL) coordinates to eliminate vertical Doppler shifting. In this frame, a finescale strain peak at $\omega_{SL} < 0.1f$ was isolated from the internal-wave band ($\omega_{SL} \geq f$), implying vortical-mode aspect ratios $k/m < 0.1f/N$ and horizontal wavelengths $\sim O(10\text{ km})$. Such low aspect ratios have almost no dynamic flow signature (passive density finestructure or layering). Finescale shear signals were centered on $\omega_{SL} \sim f$ with horizontal Doppler smearing around f consistent with aspect ratio $k/m \sim 0.1f/N$ near-inertial waves. Pinkel showed that vortical-mode strain was four orders of magnitude larger than normalized vortical-mode vertical vorticity ζ/f , and that internal-wave relative vorticity was two orders of magnitude larger than vortical-mode relative vorticity. While Pinkel's measurements did not resolve the finescale ($\lambda_z < 10\text{ m}$), these results suggest that the subinertial energy ratio attributed to vortical mode by Polzin et al. (2003) might be a Doppler-smeared admixture of subinertial density layering and finescale near-inertial shear rather than a single vortical-mode source. If this interpretation is correct, Polzin et al. would have overestimated vortical-mode shear and, since Polzin and Ferrari (2004) used these shears to infer vortical-mode stirring, this too would have been overestimated. Neither of these observational studies tested nonlinear alternatives. While anisotropic stratified turbulence is often assumed to be associated with potential vorticity finestructure (vortical motion), and most model simulations are initialized with potential vorticity anomalies, this is not necessary for a forward energy cascade, as, for example, in a broadband internal-wave field (McComas and Müller 1981; Henyey et al. 1986). This issue will be revisited in section 5b.

This paper argues that these submesoscale $[(f^3/\varepsilon)^{1/2} < k < (N^3/\varepsilon)^{1/2}]$ and finescale $[(fN^2/\varepsilon)^{1/2} < m < (N^3/\varepsilon)^{1/2}]$ wavenumber bands represent an anisotropic turbulent forward energy cascade in horizontal wavenumber k (point 4 above), which transitions into isotropic turbulence and density overturning above the Ozmidov wavenumber. Thus, geophysical isotropic and anisotropic stratified turbulence

are manifestations of the same forward energy cascade to dissipation.

Section 2 lays out dimensional scaling for isotropic and anisotropic turbulence spectra, with the core breakthrough of inferring the vertical wavenumber m spectra for anisotropic stratified turbulence for $m < m_O = k_O$ described in section 2c. Figures cited in section 3 describe the unified vertical and horizontal wavenumber model spectra and compare them to observations. After a summary in section 4, section 5 discusses implications for energy pathways, potential-vorticity-carrying finestructure, mixing efficiency, shear dispersion, and observational and numerical testing. Section 6 provides concluding remarks. Table 1 lists the fundamental dimensional variables used in this study. Table 2 lists derived dimensional variables. Table 3 lists nondimensional variables. Table 4 lists horizontal wavenumber k , vertical wavenumber m , and straining frequency u_h spectral forms for horizontal shear u_h , vertical shear $u_z \sim (m/k)u_h$, vertical divergence $w_z \sim u_h$, horizontal buoyancy gradient b_h , vertical buoyancy gradient $b_z \sim (m/k)b_h$, and horizontal strain $\chi_h = \int u_h dt$.

2. Dimensional spectral scaling

Dimensional scaling and dynamical constraints will be used to recreate observed spectral slopes (Fig. 1), assuming a uniform energy cascade rate ε in horizontal wavenumber k (Table 1) above and below the Ozmidov wavenumber as suggested by Klymak and Moum's (2007) trans-Ozmidov wavenumber spectra.

For a stationary turbulent cascade with source wavenumber k_S well separated from the dissipative sink wavenumber, the dissipation rate ε is the preferred variable for characterizing turbulence strength since it is invariant with wavenumber k , following classic stationary homogeneous turbulence arguments (Kolmogorov 1941; Batchelor 1953). As a normalized version of the dissipation rate ε , the buoyancy Reynolds number $\text{Re}_b = \varepsilon/(\nu N^2)$ is also invariant with wavenumber, but Reynolds number $\text{Re} = u/(\nu k)$ ($= 1$ at k_K and $= \text{Re}_b$ at k_O) is not. Nor are horizontal shears u_h or energies. While turbulent kinetic energy (TKE) is also an integral quantity, it is sensitive to the source wavenumber k_S for the turbulent cascade, that is, $\text{TKE} \sim (\varepsilon/k_S)^{2/3}$, so is not a reliable invariant. The gradient Froude number $\delta_N = u_z/N$ proves to be invariant in the anisotropic stratified turbulence band $k < k_O$ but not the isotropic turbulence band ($k_O < k < k_K$).

Dynamical considerations suggests three regimes: (i) isotropic turbulence between the Ozmidov and Kolmogorov wavenumber $[k_O < k < k_K = (\varepsilon/\nu^3)^{1/4}]$ where $u_h \sim u_z > N$ (gradient Froude number $\delta_N = u_z/N > 1$) and the energy cascade is downscale (section 2a), (ii) anisotropic stratified

TABLE 2. Derived dimensional variables. The Kolmogorov wavenumber $k_K = m_K$ is the upper bound and the Ozmidov $k_O = m_O$ the lower bound for isotropic turbulence, while the Ozmidov wavenumber $k_O = m_O$ is the upper bound and Coriolis wavenumbers k_f and $m_f \sim m_c$ the lower bound for anisotropic stratified turbulence. Horizontal shear u_h defines the evolution rate or straining frequency of the turbulence both above and below the Ozmidov wavenumber. The normalized horizontal buoyancy gradient b_h/N^2 is equivalent to the isopycnal slope $s = \xi_h$ and normalized vertical buoyancy gradient b_z/N^2 is equivalent to the vertical strain ξ_z in the anisotropic stratified turbulence band $k < k_O$.

Variable	Description	Scaling	Units
$k_B = m_B = L_B^{-1}$	Bachelor wavenumber	$[\varepsilon/(\nu\kappa^2)]^{1/4}$	rad m^{-1}
$k_K = m_K = L_K^{-1}$	Kolmogorov wavenumber	$(\varepsilon/\nu^3)^{1/4}$	rad m^{-1}
$k_O = m_O = L_O^{-1}$	Ozmidov wavenumber	$(N^3/\varepsilon)^{1/2}$	rad m^{-1}
k_f	Horizontal Coriolis wavenumber	$(f^3/\varepsilon)^{1/2}$	rad m^{-1}
$m_f \sim m_c$	Vertical Coriolis wavenumber \sim internal-wave rolloff wavenumber	$(fN^2/\varepsilon)^{1/2}$	rad m^{-1}
$k_S > k_f$	Turbulent source wavenumber	—	rad m^{-1}
$u_h = ku$	Horizontal shear	$\varepsilon^{1/3}k^{2/3}$	s^{-1}
$u_z = mu = \partial u/\partial z$	Vertical shear	$(m/k)u_h$	s^{-1}
w_z	Vertical divergence	$\varepsilon^{1/3}k^{2/3}$	s^{-1}
b	Buoyancy	$N^2\xi$	m s^{-2}
b_h/N^2	Normalized horizontal buoyancy gradient	$N^{-1}\varepsilon^{1/3}k^{2/3}$	Unitless
$b_z/N^2 = (m/k)b_h/N^2$	Normalized vertical buoyancy gradient	—	Unitless
$\chi_h = \int u_h dt$	Horizontal strain	—	Unitless
KE \sim HKE	Kinetic energy	u^2	$\text{m}^2 \text{s}^{-2}$
APE	Available potential energy	$b^2/N^2 \sim N^2\xi^2$	$\text{m}^2 \text{s}^{-2}$
TKE	Turbulent kinetic energy	$(\varepsilon/k_s)^{2/3} \sim \varepsilon/f$	$\text{m}^2 \text{s}^{-2}$
II	Potential vorticity	fN^2	s^{-3}

turbulence between the Coriolis and Ozmidov wavenumber [$\sim k_f < k < k_O$ where Coriolis wavenumber $k_f \sim (f^3/\varepsilon)^{1/2}$ corresponds to horizontal shears comparable to the Coriolis frequency ($u_h \sim f$)] where $f < u_h < N$ (Rossby number $\delta_f = u_h/f > 1$, $\delta_N \equiv \text{Fr} = u_z/N \sim 1$) and the energy cascade is downscale (sections 2b and 2c), and (iii) baroclinic balanced turbulence below the Coriolis wavenumber ($k < k_f$) where $u_h < f$ ($\delta_f = u_h/f < 1$, $\delta_N < 1$) with an inverse or upscale energy cascade (section 2d). A forward energy cascade for $k > k_f$ and inverse cascade for $k < \sim k_f$ might produce a spectral gap near $k \sim k_f$ if these wavenumbers are not continuously replenished by finescale instabilities. However, finescale internal waves dominate this band so will likely obscure this feature. Since quasigeostrophic turbulence is not part of the forward energy cascade, it will not be considered in any detail here.

a. Isotropic turbulence

Dimensional arguments are well known for stationary homogeneous isotropic turbulence (ISO) scales and spectra that depend on the turbulent kinetic energy dissipation rate ε , background buoyancy frequency N , molecular kinematic viscosity ν (and molecular scalar diffusivity κ), and isotropic wavenumber $k \sim m > k_O$ (Table 1; Kolmogorov 1941; Batchelor 1953; Ozmidov 1965; Tennekes and Lumley 1972; Thorpe 2005). These familiar arguments are reviewed to set the stage for scaling for anisotropic stratified turbulence below the Ozmidov wavenumber k_O (sections 2b,c).

Dimensional scaling implies that the Ozmidov (1965) wavenumber $k_O \sim L_O^{-1} \sim (N^3/\varepsilon)^{1/2}$ is the lowest bounding wavenumber for isotropic turbulence. The corresponding time scale is N^{-1} . The uppermost bounding wavenumber for turbulent shear is the Kolmogorov (or viscous) wavenumber $k_K \sim L_K^{-1} \sim (\varepsilon/\nu^3)^{1/4}$. Viscosity suppresses shear on time scale $(\nu/\varepsilon)^{1/2}$. Provided these bounding wavenumbers are sufficiently separated, that is, $k_K/k_O \sim (\varepsilon/\nu N^2)^{3/4} \sim \text{Re}_b^{3/4} \gg 1$, variances at intermediate wavenumbers $k_O \ll k \ll k_K$ are insensitive to N and ν so the shear spectra can be expressed on dimensional grounds solely in terms of the energy cascade (or dissipation) rate ε and wavenumber k , that is, $S[u_h](k) \sim \varepsilon^{2/3}k^{1/3}$ with a $+1/3$ spectral slope, corresponding to a $-5/3$ spectral slope for energy variables in this inertial subrange. The time-scale ratio $t_K/t_O \text{Re}_b^{1/2}$.

Above the Kolmogorov wavenumber and below the Batchelor (1959) wavenumber $k_B \sim L_B^{-1} \sim (\varepsilon/\kappa^2\nu)^{1/4}$,

TABLE 3. Nondimensional variables.

Variable	Description	Definition
δ_f	Rossby number (Ro)	u_h/f
δ_N	Gradient Froude number (Fr)	u_z/N
Re_b	Buoyancy Reynolds number	$\varepsilon/(\nu N^2)$
Re	Reynolds number	$u/(\nu k)$
R_E	Energy ratio	HKE/APE
R_{Lnl}	Nonlinear dynamic length-scale ratio	$Nk/(u_h m)$
R_{Ll}	Linear dynamic length-scale ratio (Burger number)	$Nk/(fm)$

TABLE 4. Anisotropic stratified and isotropic turbulence horizontal wavenumber k , vertical wavenumber m , and straining frequency u_h spectra for horizontal shear u_h , vertical shear u_z , vertical divergence w_z , normalized horizontal buoyancy gradient b_h/N^2 , normalized vertical buoyancy gradient b_z/N^2 , and horizontal strain $\chi_h = \int u_h dt$.

Variable	ANISO k	ISO k	ANISO m	ISO m	ANISO u_h	ISO u_h
u_h	$\varepsilon^{2/3} k^{1/3}$	$\varepsilon^{2/3} k^{1/3}$	$N^{-4} \varepsilon^2 m^3$	$\varepsilon^{2/3} m^{1/3}$	u_h	u_h
$u_z \sim (m/k) u_h$	$N^2 k^{-1}$	$\varepsilon^{2/3} k^{1/3}$	$N^2 m^{-1}$	$\varepsilon^{2/3} m^{1/3}$	$N^2 u_h^{-1}$	u_h
$w_z \sim u_h$	$\varepsilon^{2/3} k^{1/3}$	$\varepsilon^{2/3} k^{1/3}$	$N^{-4} \varepsilon^2 m^3$	$\varepsilon^{2/3} m^{1/3}$	u_h	u_h
b_h/N^2	$N^{-2} \varepsilon^{2/3} k^{1/3}$	$N^{-2} \varepsilon^{2/3} k^{1/3}$	$N^{-6} \varepsilon^2 m^3$	$N^{-2} \varepsilon^{2/3} m^{1/3}$	$N^{-2} u_h$	$N^{-2} u_h$
b_z/N^2	k^{-1}	$N^{-2} \varepsilon^{2/3} k^{1/3}$	m^{-1}	$N^{-2} \varepsilon^{2/3} m^{1/3}$	u_h^{-1}	$N^{-2} u_h$
$\chi_h \sim \xi_z$	k^{-1}	$N^{-2} \varepsilon^{2/3} k^{1/3}$	m^{-1}	$N^{-2} \varepsilon^{2/3} m^{1/3}$	u_h^{-1}	$N^{-2} u_h$

the spectrum for scalars with molecular diffusivities $\kappa < \nu$ ($\nu = 10^{-6} \text{ m}^2 \text{ s}^{-1}$ and $\kappa = 1.4 \times 10^{-7} \text{ m}^2 \text{ s}^{-1}$ for temperature, $1.1 \times 10^{-9} \text{ m}^2 \text{ s}^{-1}$ for salinity in the ocean) is controlled by the shear at the Kolmogorov wavenumber $(\nu/\varepsilon)^{1/2}$, yielding a scalar-gradient spectrum of the form $\chi(\nu/\varepsilon)^{1/2} k$, where χ is the scalar variance dissipation rate. The time-scale ratio $t_k/t_B = 1$ where $t_B = (\kappa k_B^2)^{-1}$ is the scalar diffusion time at the Batchelor wavenumber.

b. Horizontal wavenumber k dependence in anisotropic stratified turbulence band

For $k < k_O$, vertical and horizontal wavenumber spectra have different spectral slopes (Fig. 1). Only horizontal wavenumber k gradient spectra exhibit a $+1/3$ slope, so it will be assumed that the isotropic turbulence spectral scaling for $k > k_O$ extends below k_O in horizontal wavenumber k , while vertical wavenumber spectra must be treated separately because of the influence of stratification (section 2c). We propose that the $k^{1/3}$ horizontal wavenumber spectra observed at wavenumbers below the Ozmidov wavenumber in the ocean and atmosphere (Ewart 1976; Gage 1979; Nastrom and Gage 1985; Klymak and Moum 2007; Holbrook et al. 2013) represents a uniform turbulent energy cascade in horizontal wavenumber k that depends only on a cascade rate ε' and horizontal wavenumber k . Because (i) Klymak and Moum observed no change in their horizontal wavenumber k spectral slope or level across the Ozmidov wavenumber and (ii) a downscale energy cascade is inferred below the Ozmidov wavenumber (Lindborg and Cho 2000; Waite and Bartello 2004; Lindborg 2006; Poje et al. 2017), we equate the energy cascade rate below the Ozmidov wavenumber ε' to the dissipation rate above the Ozmidov wavenumber associated with isotropic turbulence ε ($\varepsilon \sim \varepsilon'$), that is, assume that the source for isotropic turbulence lies in the anisotropic stratified turbulence band (ANISO) at $k \ll k_O$. If this were not the case, there would be accumulation or depletion of variance at intermediate k_O , which Klymak and Moum did not observe. The Klymak and Moum (2007) observations are unique in spanning above and below k_O ,

so this assumption should be viewed with caution until it can be confirmed with additional measurements.

From this assumption, as with isotropic turbulence, the horizontal wavenumber spectrum for horizontal shear will be of the form $S[u_h](k) \sim \varepsilon^{2/3} k^{1/3}$ (Dewan 1997; Billant and Chomaz 2001) below the Ozmidov wavenumber and above a Coriolis wavenumber $k_f \sim (f^3/\varepsilon)^{1/2}$ where the Coriolis term does not inhibit horizontal nonlinearity (Lindborg 2005). Thus, the Coriolis wavenumber k_f is taken to represent the lower bounding wavenumber for anisotropic stratified turbulence. The ratio of the bounding horizontal wavenumbers, that is, the bandwidth, for this anisotropic stratified turbulence band is $k_O/k_f \sim (N/f)^{3/2}$, independent of cascade rate ε , approaching 1 as $N \downarrow f$ as in abyssal waters and at high latitudes, implying that anisotropic stratified turbulence will be most readily observed in the mid- and high-latitude pycnocline. The u_h spectrum is identical to that for horizontal Froude number u_h/N , which was used as a defining state variable by Billant and Chomaz (2001) and Lindborg (2006) following Lilly (1983), though it is not invariant with wavenumber k . Because available potential energy (APE) $\sim b^2/N^2$ is expected to scale in the same way as kinetic energy (KE) $S[\text{KE}](k) \sim k^{-2} S[u_h](k)$, the horizontal wavenumber spectrum for normalized horizontal buoyancy gradient $b_h/\langle b_z \rangle = kb/N^2$ scales as $S[b_h/\langle b_z \rangle](k) \sim N^{-2} \varepsilon^{2/3} k^{1/3}$, consistent in form with that used by Klymak and Moum (2007), $S[T_H/\langle T_z \rangle](k) = 2\gamma C_T N^{-2} \varepsilon^{2/3} k^{1/3}$, where $\gamma = 0.2$ and $C_T = 0.4$ from Batchelor (1959); note that, as a cautionary example, the combined “ $O(1)$ scaling” in this case is 0.08. The ratio b_h/N^2 is the square root of the horizontal Cox number $Cx_h = \langle b_h^2 \rangle / \langle b_z \rangle^2$ and can be equated with isopycnal slope s for $b_h/N^2 < 1$, which holds in the anisotropic stratified turbulence band ($k < k_O$). For isotropic turbulence, vertical and horizontal Cox numbers are identical, $Cx_h \sim Cx_z = \langle b_z^2 \rangle / \langle b_z \rangle^2 \sim Cx = \langle (\nabla b)^2 \rangle / \langle b_z \rangle^2$. Horizontal wavenumber k spectra are listed in Table 4.

c. Vertical wavenumber m dependence in ANISO

This section will construct the m^{-1} spectrum in the decade below the Ozmidov wavenumber $m < m_O = k_O$

by finding a relationship between m and k in the saturated band [(5)]. This is the core new contribution of this paper. Stratification dependence arises for vertical wavenumber m because N suppresses isotropy. To find this dependence for $k_f < k < k_O$, corresponding to $f < u_h < N$, nonlinear conservation of horizontal momentum can be expressed in a water-following or Lagrangian frame as

$$\frac{\partial u_z}{\partial t} + u_h u_z + w_z u_z \sim b_h \quad (1)$$

by analogy to thermal wind where buoyancy $b \sim N^2 \xi$ and isopycnal displacement ξ for $k < k_O$. The Coriolis term is neglected because $u_h > f$. The assumed hydrostatic balance $p_z \sim b$, where p is reduced pressure, will break down as $k \uparrow k_O$ and $u_h \uparrow N$. In the nonlinear ($u_h > f$) regime, $\partial/\partial t$ will scale as the straining or advective frequency u_h and continuity requires that vertical divergence $w_z \leq u_h$ since u_h is horizontal shear and not horizontal divergence, so that all three terms in the left-hand side of (1) are smaller than or scale as $u_h u_z$, reducing (1) to a gradient-wind-like balance

$$u_h u_z \sim b_h \Rightarrow u_h m u \sim k b. \quad (2)$$

Balance (2) can be rearranged to express the energy ratio $R_E = \text{KE}/\text{APE}$, where $\text{KE} \sim \text{HKE} \sim u^2$ and $\text{APE} \sim b^2/N^2 \sim N^2 \xi^2$, in terms of either (i) an aspect ratio k/m or (ii) a nonlinear dynamic length-scale ratio $R_{Lnl} = (Nk)/(u_h m)$

$$R_E = \frac{\text{HKE}}{\text{APE}} \sim \frac{N^2 k^2}{u_h^2 m^2} = R_{Lnl}^2, \quad (3)$$

where horizontal shear or straining frequency $u_h = ku$ has replaced the Coriolis frequency f of the customary linear dynamic length-scale ratio or Burger number $R_{Ll} = Nk/(fm) = \delta_f/\delta_N = \delta_f R_{Lnl}$. For a more rigorous, though more restrictive, scaling of the equations of motion, the reader is referred to Billant and Chomaz (2001).

We assume that $R_{Lnl}^2 = R_E = \text{HKE}/\text{APE} \sim O(1)$ invariant with horizontal wavenumber k . The choice of $R_{Lnl} \sim 1$ is also explicable by recognizing that this ratio is analogous to the continuum ($f \ll \omega \ll N$) linear internal-wave dispersion relation $Nk/(\omega m)$ with shearing frequency u_h replacing the intrinsic frequency ω . The R_E invariance is supported by u , v , and T sharing the same $-5/3$ spectral slope (Nastrom and Gage 1985) but is likely to break down for $u_h \sim f$ ($k \downarrow k_f$) and $u_h \sim N$ ($k \uparrow k_O$). Equipartition of KE and APE is also found in isotropic turbulence ($k > k_O$). Higher-aspect-ratio motions with $\text{HKE}/\text{APE} > 1$ are subject to zigzag instability (Billant and Chomaz 2000), analogous to barotropic instability in balanced flows, likewise implying a tendency toward $R_E = \text{HKE}/\text{APE} \sim O(1)$.

Assuming $\text{HKE}/\text{APE} \sim O(1)$, (3) implies

$$m^2 \sim \left(\frac{\text{APE}}{\text{HKE}} \right) \frac{N^2 k^2}{u_h^2} \sim \frac{N^2 k^{2/3}}{\varepsilon^{2/3}}, \quad (4)$$

which can be rearranged to

$$m \sim \frac{Nk}{u_h} \sim \frac{Nk^{1/3}}{\varepsilon^{1/3}} \quad (5)$$

for $f \ll u_h \ll N$, corresponding to $(f^3/\varepsilon)^{1/2} \ll k \ll (N^3/\varepsilon)^{1/2}$. This expression is equivalent to $m \sim N/u$ (Billant and Chomaz 2001; Lindborg 2006) since $u \sim \varepsilon^{1/3} k^{-1/3}$ on dimensional grounds (Taylor 1935). The aspect ratio k/m varies smoothly from ~ 1 isotropy at $k \sim k_O$ to $\sim f/N$ for $k \sim k_f$ ($u_h \sim f$). The ratio of bounding vertical wavenumbers for the anisotropic stratified turbulence band $m_O/m_f \sim (N/f)^{1/2}$, independent of cascade rate ε . For $k \ll k_O$, the model is consistent with the $u_h/N \ll 1$, $u_z/N \sim O(1)$ spectrum found theoretically and numerically by Billant and Chomaz (2001) and Lindborg (2006), but extends to $u_h/N \sim O(1)$ at the transition to isotropic turbulence ($k \sim k_O$). They found $u_z/N \sim O(1)$ so that vertical length scale $\ell_z = m^{-1} \sim u/N$ and $R_E \sim O(1)$ while here, invariants ε , N , and f are used along with $R_E = R_{Lnl} \sim O(1)$ to arrive at $u_z/N \sim O(1)$, $m \sim N(k/\varepsilon)^{1/3}$ and a spectral representation, but the end results are equivalent. Riley et al. (1981), Lilly (1983), and Laval et al. (2003) assumed $m \ll N/u$ and aspect ratio $m/k \sim O(1)$, neither of which holds in the anisotropic stratified turbulence regime described here.

The corresponding vertical wavenumber m spectrum for buoyancy-frequency-normalized shear (or gradient Froude number) $\delta_N = u_z/N$ is the saturated spectrum

$$S[\delta_N](m) \sim \frac{m^2}{N^2 k^2} S[u_h][k(m)] \frac{dk}{dm} \sim m^{-1} \quad (6)$$

(Dewan 1997), as found numerically by Lindborg (2006) and Brethouwer et al. (2007). This is independent of cascade rate ε . It is also the spectrum for vertical strain $\xi_z = b_z/N^2$ for $m_f < m < m_O$ (Fig. 1b). A consequence of this m^{-1} spectrum is that $u_z/N \sim O(1)$ over the vertical wavenumber band $m_c < m < m_O$ so that the buoyancy wavenumber $m_b = N/u$ used in some of the stratified turbulence literature (e.g., Riley and deBruynKops 2003; Almalkie and de Bruyn Kops 2012) is not well constrained. While not consistent with the $\text{KE}/\text{APE} \sim O(1)$ assumption here, Polzin et al.'s (2003) finding HKE/APE decreasing with vertical wavenumber for $m > m_c$ might be explicable as a wavenumber-varying admixture of anisotropic stratified turbulence and near-inertial waves as might arise from averaging lognormal distributions of finescale internal waves (E, m_c).

Dimensional scaling recovers the cascade rate ε from its spectral representations $S[E](k)dk/dt$ and $S[E](m)dm/dt$, where the evolution of the wavenumbers is expressed in terms of the geometrical-optics approximation, $dk/dt = -kdu/dx - \ell dv/dx - mdw/dx \sim ku_h \sim k^2u$ and $dm/dt = -kdu/dz - \ell dv/dz - mdw/dz \sim mu_h \sim kmu$ (Lighthill 1978), for local interactions. Vertical and horizontal terms in both equations are of the same order of magnitude. This indicates that a local time rate of change $u_h = (k^2\varepsilon)^{1/3}$ applies to both horizontal and vertical wavenumbers.

d. Vertical wavenumber m dependence for $k < k_f$

In this section, the vertical wavenumber m is inferred below the Coriolis wavenumber assuming a cascade for $u_h < f$. If energy cascades uniformly at rate ε'' for $k < k_f \sim (f^3/\varepsilon'')^{1/2}$, equivalent to $u_h < f$ ($\delta_f = \text{Ro} < 1$), then $S[u_h](k) \sim \varepsilon''^{2/3}k^{1/3}$ and thermal wind implies

$$fu_z \sim b_h \Rightarrow fmu \sim kb \quad (7)$$

by analogy to (2). Again assuming an invariant energy ratio $\text{HKE}/\text{APE} \sim O(1)$ or dynamic length-scale ratio $Nk/(fm) \sim O(1)$ (Charney 1971)

$$m^2 \sim \left(\frac{\text{APE}}{\text{HKE}}\right) \frac{N^2}{f^2} k^2 \sim \frac{N^2}{f^2} k^2 \quad (8)$$

can be rewritten as

$$m \sim \frac{Nk}{f} \quad (9)$$

so that $S[u_h](m) \sim (f/N)^{1/3}\varepsilon''^{2/3}m^{1/3}$ and $S[\text{HKE}](m) \sim (N/f)^{5/3}\varepsilon''^{2/3}m^{-5/3}$, with similar dependence on k and ε'' as in the isotropic turbulence regime. However, the energy cascade is expected to be upscale for $u_h \ll f$; Lindborg (2005) reported an upscale, or inverse, cascade for $u_h < 0.1f$. Thus, the cascade rate ε'' need not be the same as ε for $k > k_f$. The upscale cascade could be made up of weakly nonlinear balanced motions or internal gravity waves. The divergence in transfer rate near $k \sim k_f$ might lead to a spectral gap if this band is not continually replenished. Finescale internal waves dominate these scales and therefore may confound identification of the simple turbulent dimensional scaling used here, but spectral transfer rates might be able to isolate the divergence in horizontal wavenumber. There will also be a change of spectral dependence at the transition to 2D turbulence where $m \sim H^{-1}$, so that m is no longer compliant and the energy ratio R_E no longer constant. While included for completeness, there are enough uncertainties in interpretation that the $k < k_f$ band will not be explored further here.

3. Unified turbulence spectrum

This section brings together the pieces of section 2 to construct spectra in horizontal wavenumber k (section 3b), straining frequency u_h (section 3c), and vertical wavenumber m (section 3d). These are then compared with observations (section 3e). Horizontal wavenumber k , vertical wavenumber m , and straining frequency u_h spectra for anisotropic and isotropic turbulence are listed in Table 4.

a. Wavenumbers and frequencies

Anisotropic and isotropic turbulence ranges for horizontal wavenumber k , vertical wavenumber m , and straining frequency u_h are shown in Fig. 2. Turbulent horizontal wavenumbers k range from the Coriolis wavenumber $k_f \sim (f^3/\varepsilon)^{1/2}$ below the Ozmidov wavenumber $k_O = (N^3/\varepsilon)^{1/2}$ to the Kolmogorov wavenumber $k_K = (\varepsilon/\nu^3)^{1/4}$ above the Ozmidov. Corresponding vertical wavenumbers m are associated with the saturated spectrum band $m_c \sim m_f < m < m_O$ (e.g., Garrett et al. 1981) and isotropic turbulence band $m_O < m < m_K$ (Fig. 2a). For midlatitude $f = 10^{-4} \text{ rad s}^{-1}$, upper pycnocline $N = 10^{-2} \text{ rad s}^{-1}$, and buoyancy Reynolds numbers $\text{Re}_b = \varepsilon/(\nu N^2) = 500$ and 5000 (diapycnal diffusivities $K = \gamma \text{Re}_b \nu = 10^{-4} \text{ m}^2 \text{ s}^{-1}$ and $10^{-3} \text{ m}^2 \text{ s}^{-1}$ where $\gamma = -\langle w'b' \rangle/\varepsilon$ is the mixing coefficient), $k_f^{-1} \sim 200\text{--}700 \text{ m}$, and horizontal wavenumber k spans more than six decades and vertical wavenumber m four decades. Vertical wavenumbers m vary more weakly ($m \sim k^{1/3}$) in the anisotropic stratified turbulence band so that the aspect ratio k/m goes smoothly from $\sim O(1)$ isotropy at $k = k_O$ to $\sim O(f/N)$ layered flows as $k \downarrow k_f$. Bandwidths are broader in the low- and midlatitude pycnocline due to higher N . Straining or advective frequencies $u_h \sim \varepsilon^{1/3}k^{2/3}$ lie in the internal-wave band ($f < u_h < N$) for anisotropic stratified turbulence while $u_h > N$ for isotropic turbulence (Fig. 2b).

b. Horizontal wavenumber k spectrum

Horizontal wavenumber k spectra (Table 4) for normalized horizontal shear $\delta_f = u_h/f$ (Fig. 3a) and normalized horizontal buoyancy gradient b_h/N^2 (Fig. 3b) behave as $k^{1/3}$ above and below k_O , their levels rising and falling with dissipation rate ε (Figs. 3a,b), consistent with Klymak and Moum's (2007) T_h spectra and Nastrom and Gage (1985) $k^{-5/3}$ spectra for u , v , and T (Fig. 1a). Spectra for horizontal strain $\chi_h = \int u_h dt = u_h/u_h \sim 1$, since $t \sim u_h^{-1}$, and normalized vertical shear $\delta_N = u_z/N$ have -1 spectral slope and invariant spectral level for $k < k_O$ and $\varepsilon^{2/3}k^{1/3}$ dependence for $k > k_O$ (Figs. 3c,d; Table 4).

The Garrett and Munk (1979) model spectrum (GM), with spectral level E varying as $\varepsilon^{1/2}$ (Gregg 1989), peak

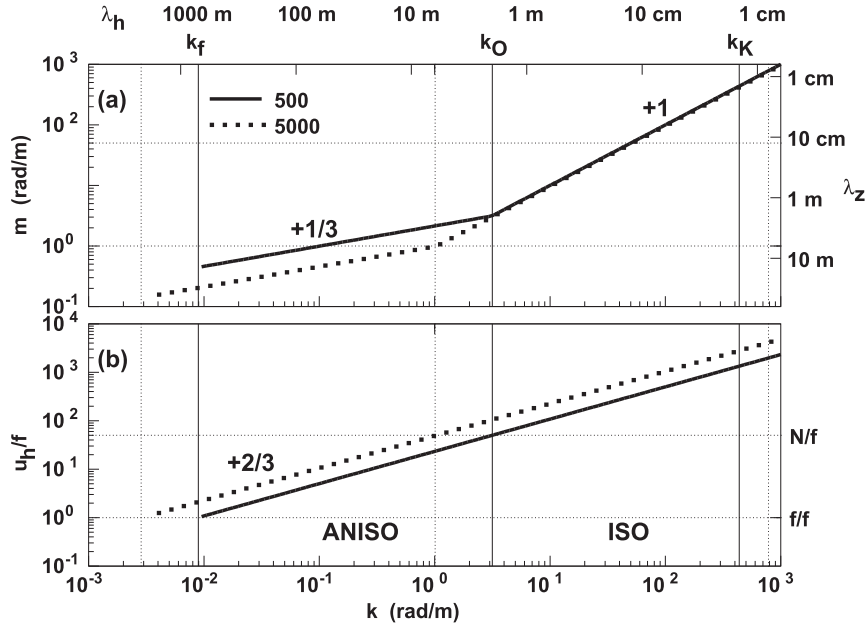


FIG. 2. Model dependence of (a) vertical wavenumber m ($= Nk^{1/3}\varepsilon^{-1/3}$ for $k_f < k < k_O$, $= k$ for $k_O < k < k_K$) and (b) normalized straining or advective frequency $\omega/f = u_h/f = k^{2/3}\varepsilon^{1/3}f^{-1}$ on horizontal wavenumber k for buoyancy frequency $N = 10^{-2} \text{ rad s}^{-1}$, Coriolis frequency $f = 10^{-4} \text{ rad s}^{-1}$, and buoyancy Reynolds numbers $\text{Re}_b = \varepsilon/(\nu N^2) = K/(\gamma\nu) = 500$ (thick solid) and 5000 (thick dotted). Slopes are indicated. Anisotropic stratified turbulence lies below the Ozmidov wavenumber ($k < k_O$), and isotropic turbulence lies above the Ozmidov wavenumber ($k > k_O$). Coriolis wavenumbers $k_f \sim (f^3/\varepsilon)^{1/2}$, Ozmidov wavenumbers $k_O = (N^3/\varepsilon)^{1/2}$, and Kolmogorov wavenumbers $k_K = (\varepsilon/\nu^3)^{1/4}$ for buoyancy Reynolds number $\text{Re}_b = 500$ (solid vertical lines) and 5000 (dotted vertical lines) as well as horizontal wavelengths λ_h are listed above the top axis of (a). Ozmidov and Coriolis wavenumbers decrease with increasing turbulent intensity Re_b , while Kolmogorov wavenumber increases. Vertical wavelengths λ_z are listed along the right axis of (a) and normalized Coriolis and buoyancy frequencies along the right axis of (b). The stratified turbulence band has straining frequencies in the internal-wave band, $f < u_h < N$.

mode number $j^* = 3$ and rolling off at vertical wavenumber $m_c = (E_{\text{GM}}/E)2\pi/(10\text{ m})$, has finite vertical wavenumber bandwidth ($m_* < m < m_c$) as well as a limited-frequency bandwidth ($f < \omega < N$), so finite horizontal wavenumber k bandwidth. GM horizontal wavenumber gradient spectra have broad maxima in horizontal wavenumber $k = m[(\omega^2 - f^2)/(N^2 - \omega^2)]^{1/2}$ spanning 1–2 decades and peaking at different k for different Re_b and different variables (thin gray dotted lines in Fig. 3): $(3\text{--}6) \times 10^{-2} \text{ rad m}^{-1}$ ($\lambda_h \sim 100\text{--}200\text{ m}$) for normalized horizontal shear δ_f , 1 rad m^{-1} ($\sim 10\text{ m}$) for horizontal buoyancy gradient b_h/N^2 (though sensitive to high wavenumbers and frequencies, which are not well constrained observationally), $3 \times 10^{-3} \text{ rad m}^{-1}$ ($\sim 5\text{ km}$) for horizontal strain, and $\chi_h = \int u_h dt$ and $10^{-3} \text{ rad m}^{-1}$ (6 km) for vertical shear δ_N . GM model levels lie below those inferred for the turbulence model spectra, but this may be because of the unknown $\sim O(1)$ scaling factor; Kunze et al. (2015) found that the GM model matched observed k^0 horizontal strain χ_h spectra near

$k \sim 10^{-2} \text{ rad m}^{-1}$ ($\lambda_h \sim 600\text{ m}$), which suggests that the anisotropic stratified turbulence model spectra (Fig. 3c) may be overestimated by an order of magnitude.

To test sensitivity to additional high-frequency variance, a near- N peak (Desaubies 1975) was added by multiplying the canonical GM model spectrum by $[N^2/(\omega^2 - N^2)]^{1/4}$ (thick gray dotted lines in Fig. 3). Only horizontal buoyancy gradient b_h/N^2 spectra (Fig. 3b) were significantly affected, becoming comparable to the turbulence model spectra around the Ozmidov wavenumber and therefore offering an alternative explanation for the Klymak and Moum (2007) T_h spectra.

c. Straining frequency u_h spectra

This section describes straining frequency u_h spectra (Table 4). Like isotropic turbulence, evolution of anisotropic stratified turbulence is governed by the straining or advective frequency $u_h = ku \sim \varepsilon^{1/3}k^{2/3}$, which represents the rate of change in a water-following frame (without vertical and horizontal Doppler-shifting by more energetic, larger-scale internal waves and mesoscale eddies,

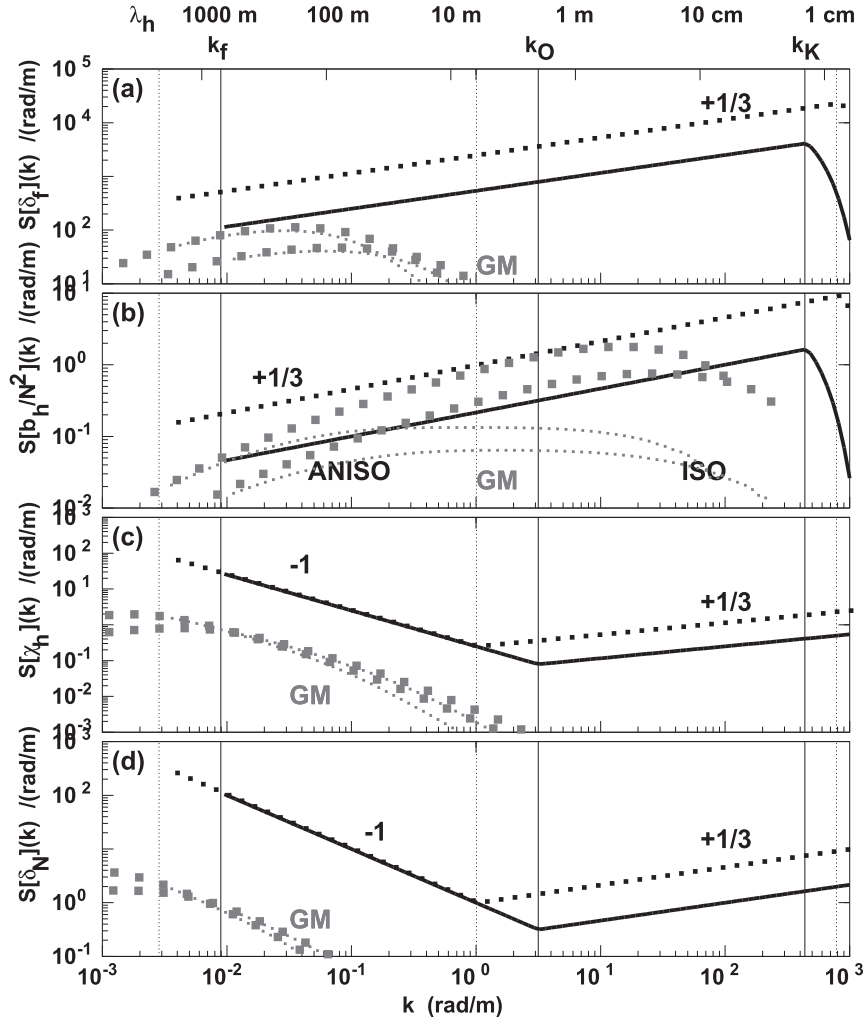


FIG. 3. Model horizontal wavenumber k spectra for (a) normalized horizontal shear $S[\delta_f](k) \sim \varepsilon^{2/3} k^{1/3} f^{-2}$ where $\delta_f = u_h/f$, (b) normalized horizontal buoyancy gradient $S[b_h/N^2](k) \sim \varepsilon^{2/3} k^{1/3} N^{-2}$, (c) horizontal strain $S[\chi_h](k)$ where $\chi_h = \int u_h dt$, and (d) normalized vertical shear $S[\delta_N](k) (\sim k^{-1}$ for $k_f < k < k_O$, $\sim \varepsilon^{2/3} k^{1/3} N^{-2}$ for $k_O < k < k_K$) where $\delta_N = u_z/N$ (Table 4) for buoyancy frequency $N = 10^{-2} \text{ rad s}^{-1}$, Coriolis frequency $f = 10^{-4} \text{ rad s}^{-1}$, and buoyancy Reynolds numbers $\text{Re}_b = \varepsilon/(\nu N^2) = 500$ (thick black solid line) and 5000 (thick black dotted line). These Re_b correspond to diapycnal diffusivities $K = \gamma \nu \text{Re}_b = 10^{-4} \text{ m}^2 \text{ s}^{-1}$ and $10 \times 10^{-4} \text{ m}^2 \text{ s}^{-1}$, respectively. Slopes are marked. Spectral levels are uncertain because of unknown $O(1)$ constants. Corresponding GM model internal-wave spectra (gray dotted curves) assume a canonical vertical wavenumber cutoff at $m_c = (E_{GM}/E)(2\pi/10 \text{ m})$. Thin gray dotted curves for the two Re_b assume the canonical frequency spectrum, while thick dotted curves add a near- N peak (section 3b).

which confounds frequency quantification in Eulerian field measurements). Straining frequencies u_h lie in the internal-wave band $f < u_h < N$ for $(f^3/\varepsilon)^{1/2} < k < (N^3/\varepsilon)^{1/2}$ as proposed by Müller et al. (1988), while $u_h > N$ for isotropic turbulence [$k > (N^3/\varepsilon)^{1/2}$] (Fig. 4). Straining frequency u_h spectra are constructed from the horizontal wavenumber spectra (Fig. 3; Table 4) using the transformation $k \sim \varepsilon^{-1/2} u_h^{3/2}$ so that $dk/du_h \sim \varepsilon^{-1/2} u_h^{1/2}$ and then $S[X][k(u_h)]dk/du_h$. This yields frequency spectra that behave as (i) $\sim u_h/f^2$ for normalized horizontal shear δ_f ,

(ii) $\sim u_h/N^2$ for horizontal buoyancy gradient b_h/N^2 , and (iii) $\sim u_h^{-1}$ for $k < k_O$ and $\sim u_h/N^2$ for $k > k_O$ for horizontal strain χ_h (Fig. 4). All these spectra have spectral levels independent of cascade rate ε as a result of the dimensional scaling and thus provide no information about turbulent dissipation rates ε . Frequency spectra for anisotropic turbulence spectra are bluer than the GM internal-wave spectra. In Fig. 4, their levels are higher than those of internal waves for normalized horizontal shear $\delta_f = u_h/f$ and horizontal strain $\chi_h = \int u_h dt$, while

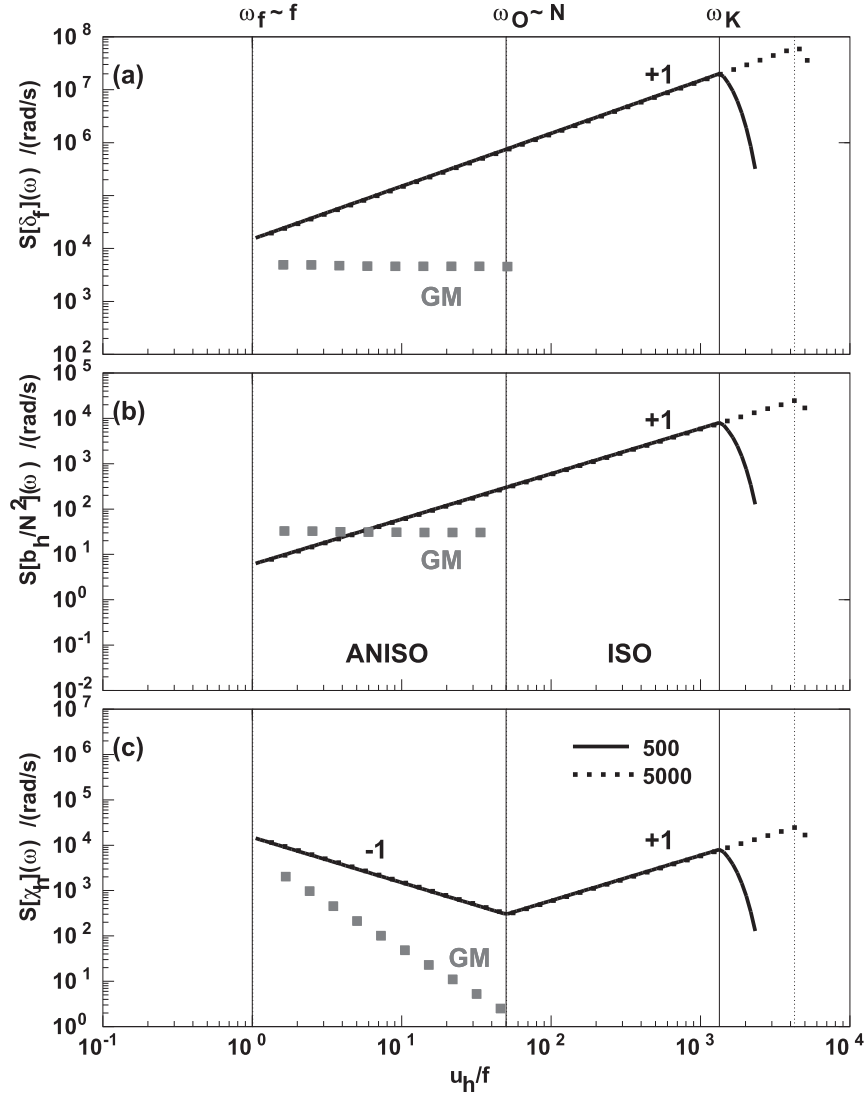


FIG. 4. Model straining frequency $\omega = u_h = ku = \varepsilon^{1/3}k^{2/3}$ spectra for (a) normalized horizontal shear $S[\delta_f](\omega) \sim \omega f^{-2}$ where $\delta_f = u_h/f$, (b) normalized horizontal buoyancy gradient $S[b_h/N^2](\omega) \sim \omega N^{-2}$, and (c) isopycnal strain $S[\chi_h](\omega)$ where $\chi_h = \int u_h dt = u_h/\omega = u_h/u_h \sim 1$ (Table 4). Thick black solid lines correspond to buoyancy Reynolds number $Re_b = \varepsilon/(\nu N^2) = 500$ and thick black dotted lines to $Re_b = 5000$. Anisotropic stratified turbulence straining frequencies lie in the internal-wave band $f < u_h < N$. Corresponding GM model spectra are redder (gray dotted lines). Spectral levels are independent of Re_b but the Kolmogorov rolloff k_K increases with ε . Stratified anisotropic turbulence horizontal shear u_h/f and isopycnal strain χ_h lie above the GM spectral levels, while normalized horizontal buoyancy gradient b_h/N^2 spectra have similar levels but have $O(1)$ constants so may be overestimated (section 3c).

horizontal buoyancy gradient b_h/N^2 shows a crossover between $\omega_f \sim f$ and $\omega_O \sim N$ (Fig. 4b). Again, this should be viewed with caution since the model spectra are based on dimensional scaling and may be overestimated (section 3b).

d. Vertical wavenumber m spectra

Vertical wavenumber m spectra for normalized vertical shear $\delta_N = u_z/N$ (Fig. 5) and normalized vertical

buoyancy gradient b_z/N^2 are identical (Table 4), closely resembling observed spectra (Fig. 1b). In the isotropic turbulence band above the Ozmidov wavenumber $m_O = k_O$, spectral slopes are $+1/3$ and levels vary as $\varepsilon^{2/3}$. In the anisotropic turbulence band below the Ozmidov wavenumber, spectral slope is -1 and spectral level invariant, consistent with observed saturated vertical wavenumber spectra for vertical shear $S[u_z](m) \sim N^2 m^{-1}$

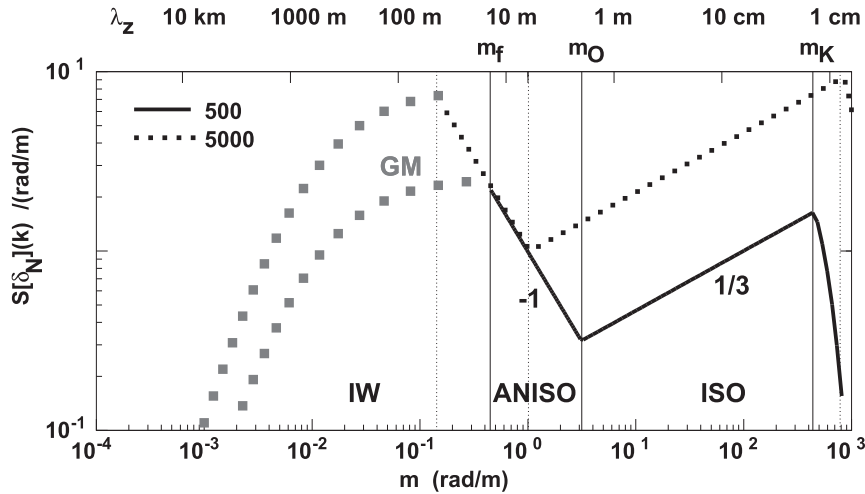


FIG. 5. Model vertical wavenumber m spectra $S[\delta_N](m)$ for normalized vertical buoyancy gradient b_z/N^2 and normalized vertical shear $\delta_N = u_z/N$ behave as $\sim m^{-1}$ for $m_c \sim m_f < m < m_O$ and $\sim \varepsilon^{2/3} m^{1/3} N^{-2}$ for $m_O < m < m_K$ (Table 4). Buoyancy Reynolds number $Re_b = 500$ correspond to the thick black solid line and $Re_b = 5000$ the thick black dotted line. Corresponding GM model spectra for peak mode number $j^* = 3$ are shown below the Coriolis vertical wavenumber $m_f \sim m_c$ as thick gray dotted curves. Coriolis vertical wavenumbers $m_f \sim (N^2/f\varepsilon)^{1/2}$, Ozmidov wavenumbers $m_O = (N^3/\varepsilon)^{1/2}$, and Kolmogorov wavenumbers $m_K = (\varepsilon/\nu^3)^{1/4}$ for buoyancy Reynolds number $Re_b = 500$ (solid vertical lines) and 5000 (dotted vertical lines) as well as vertical wavelengths λ_z are indicated above the top axis.

(Gargett et al. 1981; Fritts 1984; Fritts et al. 1988; Dewar and Good 1986; Smith et al. 1987; Gregg et al. 1993; Dewar 1997; Billant and Chomaz 2001). The gradient Froude number $\delta_N = u_z/N \sim O(1)$ in the stratified turbulence band (if $\delta_N = 2$ at m_O , then $\delta_N \sim 1.3$ at $m_c \sim m_f$), consistent with the tendency in stratified turbulence simulations (Billant and Chomaz 2001; Riley and deBruynKops 2003; Lindborg 2006; Brethouwer et al. 2007) and contrary to earlier modeling of stratified turbulence that assumed $\delta_N \ll 1$ (Riley et al. 1981; Lilly 1983; Laval et al. 2003). The Coriolis vertical wavenumber $m_f = (N/f)k_f = (f/N)^{1/2}m_O = (fN^2/\varepsilon)^{1/2}$ appears to correspond to the rolloff wavenumber m_c of the modified canonical internal-wave model spectrum (e.g., Gargett et al. 1981). GM internal waves dominate below the rolloff wavenumber $m_c \sim m_f$.

e. Comparison with observations

The spectral model compares favorably with ocean observations. Klymak and Moum (2007) displayed ocean T_h spectra for diapycnal diffusivities $K = (0.05\text{--}15) \times 10^{-4} \text{ m}^2 \text{ s}^{-1}$, corresponding to buoyancy Reynolds numbers $Re_b \sim 25\text{--}7500$. For the buoyancy frequency $N \sim 4.5 \times 10^{-3} \text{ rad s}^{-1}$, this implies dissipation rates $\varepsilon = 5 \times 10^{-10}\text{--}1.5 \times 10^{-7} \text{ W kg}^{-1}$ and Ozmidov length scales of 0.01–1.1 m. For a Coriolis frequency $f \sim 10^{-4} \text{ rad s}^{-1}$, it implies $k_f \sim 0.3\text{--}0.015 \text{ rad m}^{-1}$ ($\lambda_f \sim 20\text{--}400 \text{ m}$), which matches the lower-wavenumber bounds of their $+1/3$

spectral slope ranges. Corresponding rms velocities are $(\varepsilon/f)^{1/2} \sim 0.2\text{--}4 \text{ cm s}^{-1}$. For more typical average ocean diffusivities $K \sim 0.1 \times 10^{-4} \text{ m}^2 \text{ s}^{-1}$ and pycnocline buoyancy frequencies $N \sim 5 \times 10^{-3} \text{ rad s}^{-1}$, rms velocities associated with anisotropic stratified turbulence $(\varepsilon/f)^{1/2} \sim 1 \text{ cm s}^{-1}$ are consistent with the current fine-structure that could not be accounted for by linear internal gravity waves in the Internal Wave Experiment (IWEX) trimooring (Briscoe 1977; Müller et al. 1978). Predicted horizontal shear variances of $\sim 0.03f^2$ at 1000-m scales and $\sim 200f^2$ at 5-m scales (Fig. 3a) are also consistent with IWEX array measurements (Müller et al. 1988). At lower horizontal wavenumbers $k \sim (2\text{--}20) \times 10^{-4} \text{ rad m}^{-1}$ (horizontal wavelengths 3–30 km) in the summer Sargasso Sea pycnocline, Callies et al. (2015) reported roughly $-5/3$ spectral slopes for velocity with Rossby numbers $\delta_f = u_h/f \sim 0.5\text{--}1$ and spectral levels close to those of the GM model spectra. They partitioned these signals to internal waves based on a linear decomposition (Bühler et al. 2014) that attributes all horizontal divergence to linear internal-wave motions. Since the nonlinear anisotropic stratified turbulence described here has horizontal divergence $\sim u_h \sim w_z \sim \varepsilon^{1/3} k^{2/3}$, its variance would be misassigned to internal waves by this decomposition.

The proposed model spectra are also comparable with atmospheric aircraft data. Nastrom and Gage (1985) found a $-5/3$ spectral slope from aircraft measurements

of velocity and temperature at horizontal wavenumbers $k = (1\text{--}100) \times 10^{-5} \text{ rad m}^{-1}$ (5–500 km horizontal wavelengths) and a -3 slope at lower wavenumbers. For $f \sim 10^{-4} \text{ rad s}^{-1}$ and $N \sim 10^{-2} \text{ rad s}^{-1}$, this implies dissipation rates $\varepsilon \sim 0.25 \text{ W kg}^{-1}$, Ozmidov length scales $L_O \sim 0.5 \text{ km}$ and rms velocities $u_f \sim 10 \text{ m s}^{-1}$, which are somewhat larger than the $\sim 4 \text{ m s}^{-1}$ inferred from their spectra. Their spectra imply Rossby numbers $\delta_f \sim 1$ at 500-km horizontal wavelength and ~ 2 at 5-km wavelength, consistent with the spectral model. More recent atmospheric horizontal wavenumber spectra (Callies et al. 2014, 2016) also show $-5/3$ spectral slopes over horizontal wavenumbers $k \sim (1\text{--}50) \times 10^{-5} \text{ rad m}^{-1}$ with corresponding rms Rossby numbers $\delta_f \sim 0.5\text{--}2$. Their linear decomposition ascribed this band to internal gravity waves based on horizontal divergence and lower wavenumbers to geostrophic turbulence.

4. Summary

Taking inspiration from classic turbulence theory (e.g., Kolmogorov 1941; Batchelor 1953), dimensional scaling was used to construct a spectral model from the turbulent cascade or dissipation rate ε , background buoyancy frequency N , Coriolis frequency f , and horizontal wavenumber k (Table 1) for the decade or so below the Ozmidov (1965) wavenumber $k_O = (N^3/\varepsilon)^{1/2}$ (Figs. 3, 5), that is, at scales lying between those attributed to internal gravity waves and isotropic turbulence (vertical wavelengths $\lambda_z \sim 1\text{--}10 \text{ m}$, horizontal wavelengths $\lambda_h \sim 1\text{--}1000 \text{ m}$ in the ocean; $\lambda_z \sim 1\text{--}10 \text{ km}$ and $\lambda_h \sim 1\text{--}1000 \text{ km}$ in stratosphere). Spectral forms are listed in Table 4. Derived dimensional and nondimensional variables are listed in Tables 2 and 3, respectively. A forward energy cascade rate ε invariant in horizontal wavenumber k was assumed below as well as above the Ozmidov wavenumber $(N^3/\varepsilon)^{1/2}$ (sections 2a and 2b). To produce a vertical wavenumber m spectrum (Fig. 5), the energy ratio $R_E \sim \text{KE}/\text{APE}$, was assumed to be an $\sim O(1)$ invariant across horizontal wavenumber k (section 2c). If the finescale parameterization (McComas and Müller 1981; Henyey et al. 1986; Gregg 1989; Polzin et al. 1995) links the internal-wave field to isotropic turbulence, the spectral model described here fills in the gap between the two as a further step toward unifying this range of scales and dynamics. The model should be relevant in Earth's ocean and atmosphere, in stellar and planetary atmospheres, and in other rotating stratified fluids.

The model horizontal wavenumber k and vertical wavenumber m spectra (Figs. 3, 5; Table 4) are consistent with those observed (Fig. 1). Specifically, the model reproduces (i) the $+1/3$ gradient spectral slope in horizontal wavenumber k for horizontal buoyancy gradient b_h (Fig. 1a; Klymak and Moum 2007) and horizontal

shear u_h [equivalent to the $-5/3$ spectral slope for u , v , and T in Nastrom and Gage (1985)], with spectral levels rising and falling with the dissipation rate ε above and below k_O (Figs. 3a,b), (ii) the -1 spectral slope in vertical wavenumber m for normalized vertical shear u_z/N (Fig. 1b; Gargett et al. 1981) and vertical buoyancy gradient b_z/N^2 , with invariant spectral levels in the saturated spectrum band below the Ozmidov wavenumber (Fig. 5), and (iii) a $+1/3$ gradient spectral slope in vertical wavenumber above the Ozmidov wavenumber for these variables that rises and falls with ε (Fig. 5). Straining frequencies u_h occupy the same band as internal gravity waves ($f < u_h < N$), but frequency spectra are bluer (more positive spectral slope) than the GM model spectrum for internal waves and have invariant spectral levels (Fig. 4).

5. Discussion

Anisotropic stratified turbulence has a finite bandwidth [$\sim k_f < k < k_O$, $m_f \sim m_c < m < m_O$, $u_z \sim N$, $f < u_h \sim \omega < N$, where $k_f = (\varepsilon/f^3)^{1/2}$, $m_f = (\varepsilon/fN^2)^{1/2}$, $k_O = m_O = (N^3/\varepsilon)^{1/2}$] in the bands between internal gravity waves ($f < \omega < N$, $m < m_c$, $u_h < \omega$, $u_z < N$) and isotropic turbulence ($k_O < k \sim m < k_K$, $u_h \sim u_z > N$). In the following subsections, broader implications will be discussed for (section 5a) energy pathways, (section 5b) potential-vorticity-carrying finestructure (vortical motion), (section 5c) mixing efficiency, (section 5d) shear dispersion, (section 5e) observational, and (section 5f) numerical testing. This discussion challenges several of the author's preconceptions:

- 1) That isotropic turbulence arises from vertical shear and/or overturning instability of internal gravity waves at the Ozmidov scale (e.g., Miles 1961; Thorpe 1978; Kunze 2014), instead suggesting that isotropic turbulence is part of a forward energy cascade that can originate at horizontal wavenumbers k well below the Ozmidov wavenumber k_O where anisotropic rather than vertical internal-wave instability feeds energy into anisotropic.
- 2) That potential vorticity can only be modified by diabatic processes at molecular dissipative, that is, Kolmogorov $(\varepsilon/\nu^3)^{1/4}$ and Batchelor $[\varepsilon/(\nu\kappa^2)]^{1/4}$ wavenumbers (Ertel 1942; Polzin et al. 2003), instead finding that dissipative forcing of potential vorticity takes the form of a convolution integral in spectral space that induces potential vorticity anomalies across the anisotropic and isotropic turbulence wavenumber bands (section 5b). This indicates that turbulence will create potential-vorticity-carrying finestructure (vortical motion) in the process of dissipating.

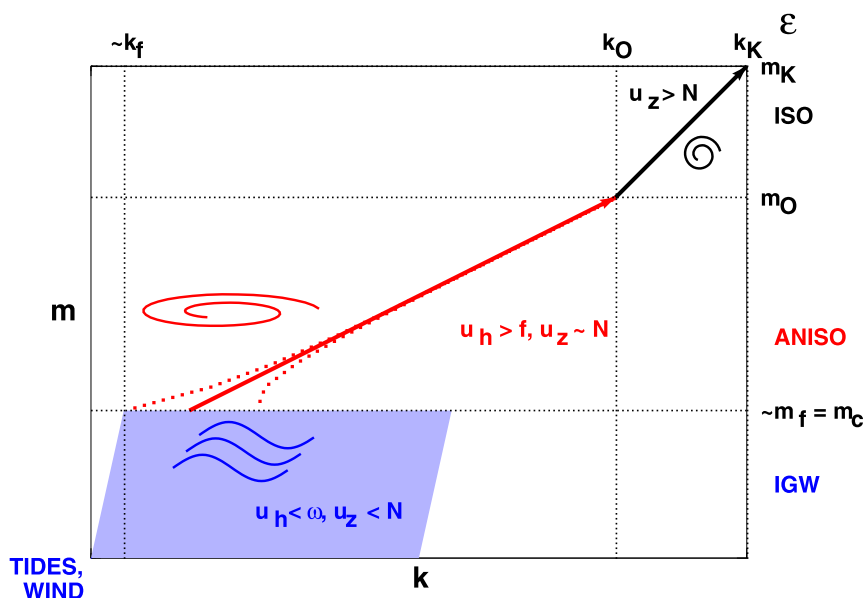


FIG. 6. Schematic showing proposed energy pathways in horizontal wavenumber k and vertical wavenumber m space from tide and wind sources in the lower-left corner to dissipation ε at the upper-right corner. The cascade rate ε is invariant across all bands to ensure no accumulation or depletion of variance at any intermediate wavenumber. Internal gravity waves ($f < \omega < N$) will have horizontal shears less than their frequencies ($u_h < \omega$) and gradient Froude number $\delta_N = u_z/N < 1$ [blue internal gravity wave (IGW); lower-left corner]. Wave-wave interactions transfer energy toward the rolloff vertical wavenumber $m_c \sim m_f = (fN^2/\varepsilon)^{1/2} = (N/f)k_f$ and low frequencies $\omega \sim f$. Anisotropic stratified turbulence at $\sim k_f < k < k_O = m_O = (N^3/\varepsilon)^{1/2}$ triggers anisotropic stratified turbulence (red ANISO; $\delta_f = u_h/f > 1$, $\delta_N \sim 1$), which continues the energy cascade, transitioning to isotropic turbulence (black ISO; upper right; $\delta_N > 1$) and density overturning at the Ozmidov wavenumber k_O and on to dissipation ε at the Kolmogorov wavenumber $k_K = m_K = (\varepsilon/\nu^3)^{1/4}$. The Coriolis wavenumber $k_f \sim (f^3/\varepsilon)^{1/2}$ corresponds to where horizontal shear $u_h \sim f$.

a. Energy pathways

Proposed energy pathways are illustrated in Fig. 6. Tides and wind feed energy into the internal-wave field at the bottom and surface boundaries. Low-mode wave energy ($m \ll m_c$) propagates vertically and horizontally to fill the stratified ocean interior, while nonlinear wave/wave interactions cascade wave energy from low to high vertical wavenumbers m and to low frequencies $\omega \sim f$ and low aspect ratios k/m (McComas and Müller 1981; Henyey et al. 1986). Internal waves are assumed to be stable ($\delta_f < 1$, $\delta_N < 1$) except intermittently at their highest wavenumbers k_f and $m_f \sim m_c$. Rather than vertical shear or convective instability of finescale internal waves ($\delta_N > 2$) directly injecting energy into isotropic turbulence at or above the Ozmidov wavenumber k_O , this paper proposes that anisotropic instability (detailed below) of $\sim f/N$ aspect ratio finescale near-inertial waves ($\delta_f > 1$) can feed energy into the low-wavenumber end of anisotropic stratified turbulence ($k \sim k_f \ll k_O$). A downscale energy cascade proceeds through the Ozmidov wavenumber $k_O = m_O$ where it transitions

to isotropic turbulence and density overturning to continue the forward cascade to molecular dissipation at the Kolmogorov wavenumber $k_K = m_K = (\varepsilon/\nu^3)^{1/4}$. The average cascade rate ε is assumed to be identical in all three domains, and identical to the turbulent dissipation rate, so that there is no accumulation or depletion of variance at any intermediate wavenumber, that is, anisotropic stratified turbulence is part of the turbulent downscale energy cascade to dissipation.

The forward energy cascade inferred in the anisotropic stratified turbulence regime in transfer spectra for atmospheric tracers (Lindborg and Cho 2000), ocean drifter arrays (Poje et al. 2017), and numerical simulations (Waite and Bartello 2004; Lindborg 2006), together with continuity in spectral slope and level across the Ozmidov wavenumber in Klymak and Moum's (2007) horizontal T_h spectra, suggests that anisotropic stratified turbulence below k_O and isotropic turbulence above k_O are manifestations of the same downscale cascade to dissipation. It further suggests that a downscale geophysical turbulent cascade can be initiated

anisotropically at source horizontal wavenumbers k_S as low as the Coriolis wavenumber $k_f \sim (f^3/\varepsilon)^{1/2}$ (Lindborg 2005), with no intervening sources or sinks between $k_S \ll k_O$ and the sink Kolmogorov wavenumber k_K . This implies turbulent energy sources at horizontal scales as large as ~ 100 m in the ocean and ~ 500 km in the atmosphere. In the stratified ocean interior, energy sources for turbulence are well established as instability of finescale near-inertial waves by the predictive skill of the finescale shear/strain parameterization for turbulent dissipation rate ε (Gregg 1989; Polzin et al. 1995; Gregg et al. 2003; Whalen et al. 2015); this parameterization is based on the energy cascade to high wavenumbers by internal-wave/wave interactions (McComas and Müller 1981; Henyey et al. 1986). Here, the transition from internal waves to turbulence is proposed to be due to horizontal ($u_h > f$) or anisotropic instability of fine-scale internal waves.

This contrasts with conventional wisdom that isotropic turbulence is generated by vertically breaking internal waves ($u_z > 2N$) injecting energy directly into the outer scales of isotropic turbulence, that is, at the Ozmidov or density-overturning scales (e.g., Kunze et al. 1990; D'Asaro and Lien 2000; Smyth et al. 2001; Mashayek et al. 2017). This convention is founded on theoretical and laboratory studies without background horizontal variability ($\partial/\partial x = 0$; e.g., Miles 1961; Thorpe 1973) for which vertical instability is the only option. However, in the ocean pycnocline, the most energetic turbulence patches have aspect ratios $\sim f/N$ and are associated with marginally unstable finescale near-inertial wave packets (Gregg et al. 1986; Marmorino 1987; Marmorino et al. 1987; Itsweire et al. 1989; Rosenblum and Marmorino 1990; Marmorino and Trump 1991; Hebert and Moum 1994; Kunze et al. 1995; Polzin 1996) with aspect ratios $k/m = (\omega^2 - f^2)^{1/2}/N = f(2\epsilon)^{1/2}/N \sim f/N$, where near-inertial frequency $\omega = f(1 + \epsilon)$ and $\epsilon = 0.1$ – 0.2 (D'Asaro and Perkins 1984). Therefore, unstable vertical shears $\delta_N = |u_z|/N > \delta_{Nc}$ will be accompanied or preceded by unstable horizontal shears $\delta_f = |u_h|/f = (k/m)(N/f)\delta_N \sim \delta_N > \delta_{fc}$ where δ_{Nc} and δ_{fc} are $O(1)$ critical thresholds for instability in the vertical and horizontal, respectively. Horizontal, or some kind of mixed anisotropic, instability would inject energy into the anisotropic stratified turbulence band at horizontal wavenumbers $k_S \sim (f/N)m_c \ll k_O$. The author is unaware of any stability theory or modeling that takes into account the horizontal structure of near-inertial wave packets with $\sim f/N$ aspect ratios.

A turbulence source at wavenumber $k_S \ll k_O$ implies a turbulent energy reservoir TKE $\sim (\varepsilon/k_S)^{2/3} \sim \varepsilon/f$, much larger than the $\sim \varepsilon/N$ of isotropic turbulence. The time scale for dissipation of energy injected at k_O is $(\varepsilon k_O^2)^{1/3} \sim O(N^{-1})$, while a lower source wavenumber

$\sim k_f$ would allow turbulence to persist for $(\varepsilon k_f^2)^{1/3} \sim O(f^{-1})$. This is consistent with observed durations of energetic $\sim f/N$ aspect ratio turbulent patches (Gregg et al. 1986; Hebert and Moum 1994). Thus, persistent turbulence patches need not be maintained by recurrent vertical instabilities but could be instigated by a single instability event.

Anisotropic stratified turbulence can exist for lower dissipation rates ε than isotropic turbulence. Isotropic turbulence requires $Re_b \gg 1$ for there to be sufficient bandwidth between the Ozmidov and Kolmogorov wavenumbers. However, anisotropic turbulence only requires there to be sufficient bandwidth between the Coriolis and Kolmogorov wavenumbers, that is, $m_K/m_f = (N/f)^{1/2} Re_b^{3/4} \gg 1$. In the pycnocline, this allows dissipation rates as much as an order of magnitude smaller to be turbulent. Assuming that $(N/f)^{3/2} Re_b > O(100)$ is sufficient for there to be anisotropic turbulent bandwidth between $m_f \sim m_c$ and m_K , then cascade rates ε as low as $10^{-11} \text{ W kg}^{-1}$ ($k_f \sim 1 \text{ rad m}^{-1}$, $k_K \sim 30 \text{ rad m}^{-1}$) and as high as $10^{-8} \text{ W kg}^{-1}$ ($k_f \sim 0.01 \text{ rad m}^{-1}$, $k_K \sim 100 \text{ rad m}^{-1}$) in the midlatitude pycnocline ($f = 10^{-4} \text{ rad s}^{-1}$, $N = 10^{-2} \text{ rad s}^{-1}$) might forward cascade to dissipation with no isotropic band between k_S and k_K . Globally, these would represent less than 10^{-2} TW integrated dissipation, or $\sim 1\%$ of tide and wind generation. If isotropic turbulence never forms, viscous damping would act anisotropically on vertical shear. There would be no isotropic Batchelor spectrum for density, but an anisotropic Batchelor spectrum would arise for passive scalars on isopycnals over $(\varepsilon/\nu^3)^{1/4} < k < [\varepsilon/(\nu\kappa^2)]^{1/4}$.

b. Anisotropic stratified turbulence and potential-vorticity-carrying finestructure

This section discusses potential vorticity generation by molecular dissipation at the end of the cascade. This occurs nonlocally in horizontal wavenumber k over the anisotropic and isotropic turbulence wavenumber bands. In the ocean interior, Ertel potential vorticity $\Pi = \nabla b \cdot (2\mathbf{\Omega} + \nabla \times \mathbf{v})$ can only be modified from its planetary value fN^2 through irreversible dissipative processes due to molecular viscosity ν and diffusivity κ

$$\frac{D\Pi}{Dt} = \nabla b \cdot \nu \nabla^2 (2\mathbf{\Omega} + \nabla \times \mathbf{v}) + (2\mathbf{\Omega} + \nabla \times \mathbf{v}) \cdot \kappa \nabla^2 (\nabla b) \quad (10)$$

(Ertel 1942; Lelong 1989). In the isotropic turbulence band that is expected to dominate gradients on the rhs of (10), planetary rotation can be neglected, $|\nabla b| \sim |b_h|$ with Fourier transform $\sim N\varepsilon^{1/3}k^{2/3}/k$, $|\nabla \times \mathbf{v}| \sim |u_h|$ with Fourier transform $\sim \varepsilon^{1/3}k^{2/3}/k$, and Laplacian $|\nabla^2| \sim |k^2|$. Thus, (10) can be approximated spectrally as a convolution

integral describing nonlocal influences across horizontal wavenumber k

$$\tilde{\Pi}_i(k) \sim \nu N \varepsilon^{2/3} \int_{-\infty}^{\infty} \left[\frac{k'^{2/3} (k - k')^2 (k - k')^{2/3}}{k'} \right] \cos \theta_r dk' + \kappa N \varepsilon^{2/3} \int_{-\infty}^{\infty} \left[\frac{k'^{2/3} (k - k')^2 (k - k')^{2/3}}{k'} \right] \cos \theta_r dk', \quad (11)$$

where θ_r represents the orientation difference between the vorticity and buoyancy-gradient vectors. Since the two integrands are identical and $\nu \gg \kappa$, the second integral prefaced by κ will be neglected and (11) simplifies to

$$\tilde{\Pi}_i(k) \sim \nu N \varepsilon^{2/3} \int_{-\infty}^{\infty} [k'^{2/3} (k - k')^{5/3}] \cos \theta_r d \log k', \quad (12)$$

where $d \log k = dk/k$. The potential vorticity Fourier transform time rate of change [(12)] is evaluated numerically, with integrands assumed to vanish for $|k'|$, $|k - k'| < k_O$ and $|k'|$, $|k - k'| > k_K$. If the buoyancy gradient and vorticity vectors are orthogonal across all wavenumbers k , as with internal gravity waves, then (12) vanishes. At the other extreme, if the vectors are parallel to each other over all k so that $\cos \theta_r = 1$, the convolution implies a rate of change $\tilde{\Pi}_i(k)/\tilde{\Pi}(k) \sim O(N)$ over the anisotropic stratified turbulence band $\sim k_f < k < k_O$ (Fig. 7), normalized by the maximal potential vorticity, which is also as a convolution integral

$$\tilde{\Pi}(k) \sim N \varepsilon^{2/3} \int [k'^{2/3} (k - k')^{-1/3}] d \log k'. \quad (13)$$

This high rate arises because the convolution integral is dominated by vorticity and buoyancy gradient interactions at $k \sim k_K$ where both are maximal. Performing the integration only over $|k'|$, $|k - k'| > k_K/2$ yields almost identical results in the anisotropic turbulence band.

Neither zero nor perfect coherence between different wavenumbers k seem likely for turbulence. Monte Carlo simulations where θ_r was chosen at random within $\{0-2\pi\}$ for each of 2000 k' generate potential vorticity anomalies of both signs at rates $\sim O(0.1N) \sim O(10f)$ at all wavenumbers in the anisotropic and isotropic turbulence bands (Fig. 7). Inferred maximal potential vorticity anomalies from (13) near the Coriolis wavenumber k_f are $\sim O(0.1fN^2)$. These may be overestimates because the vorticity and buoyancy gradient vectors are taken to be parallel to each other in (13). The relationship between these two vectors near the Kolmogorov wavenumber is uncertain.

While the analysis above is far from robust, damping at dissipative scales appears capable of producing

potential vorticity anomalies across the anisotropic and isotropic turbulence bands, consistent with Winters and D'Asaro (1994) finding a large fraction of wave energy encountering a critical layer left behind in low-wavenumber vortical motion. Since molecular dissipation is responsible for potential vorticity modification [(10)], vortical motion will only arise after the cascade reaches dissipative wavenumbers $k \sim k_K = (\varepsilon/\nu^3)^{1/4}$ and so is an end product of turbulence, like mixing. This does not address whether vortical motion is dynamically important for the energy cascade.

Some energy injected near $\sim k_f$ ($u_h \sim f$) is likely to inverse cascade to larger horizontal length scales (Lindborg 2005, 2006), as will variance left behind as turbulence decays and k_f increases. Molecular viscosity will act more rapidly to extract laminar momentum than molecular scalar diffusivity removes density anomalies, further modifying potential vorticity. Viscous decay will cause the energy ratio KE/APE to decrease and aspect ratios k/m flatten, producing subinertial density layering ($u_h \rightarrow 0$, $k/m < f/N$) with little dynamic signal like that reported by Pinkel (2014). This train of events is conjectural.

c. Mixing coefficient γ

A turbulence source at $k_S \ll k_O$ may explain why microstructure measurements in the ocean pycnocline more consistently infer mixing coefficients $\gamma = -\langle w'b' \rangle / \varepsilon \sim 0.2$ at high-buoyancy Reynolds numbers Re_b (Oakey 1982; St. Laurent and Schmitt 1999; Gregg et al. 2018; Ijichi and Hibiya 2018) than the smaller values reported in laboratory experiments (Barry et al. 2001), numerical simulations (Shih et al. 2005), and near boundaries (Davis and Monismith 2011; Lozovatsky and Fernando 2012; Bluteau et al. 2013). If turbulence is generated anisotropically at $k_S \ll k_O$ and cascades energy forward, isotropic turbulence will always arise at the Ozmidov scale away from boundaries. In contrast, laboratory tanks, numerical domains, and proximity to boundaries will suppress overturns at the largest scales as Re_b increases and the Ozmidov length scale $L_O = (\varepsilon/N^3)^{1/2} = (\nu N Re_b)^{1/2}$ exceeds the domain size, reducing turbulent buoyancy anomalies b' and fluxes $\langle w'b' \rangle$ relative to dissipation rates ε , and so lowering the mixing coefficient γ . This argument will not hold in the abyssal ocean where $N \rightarrow f$ so that $k_S \sim k_O$ and the ratio of Thorpe to Ozmidov length scales L_T/L_O is observed to regularly exceed 1 (Ijichi and Hibiya 2018), consistent with young turbulence.

d. Shear dispersion

Anisotropic stratified turbulence will contribute to shear dispersion and isopycnal diffusivity K_h

$$K_h = \langle K \chi_z^2 \rangle = \langle K \rangle \langle \chi_z^2 \rangle + \langle \delta K \delta \chi_z^2 \rangle, \quad (15)$$

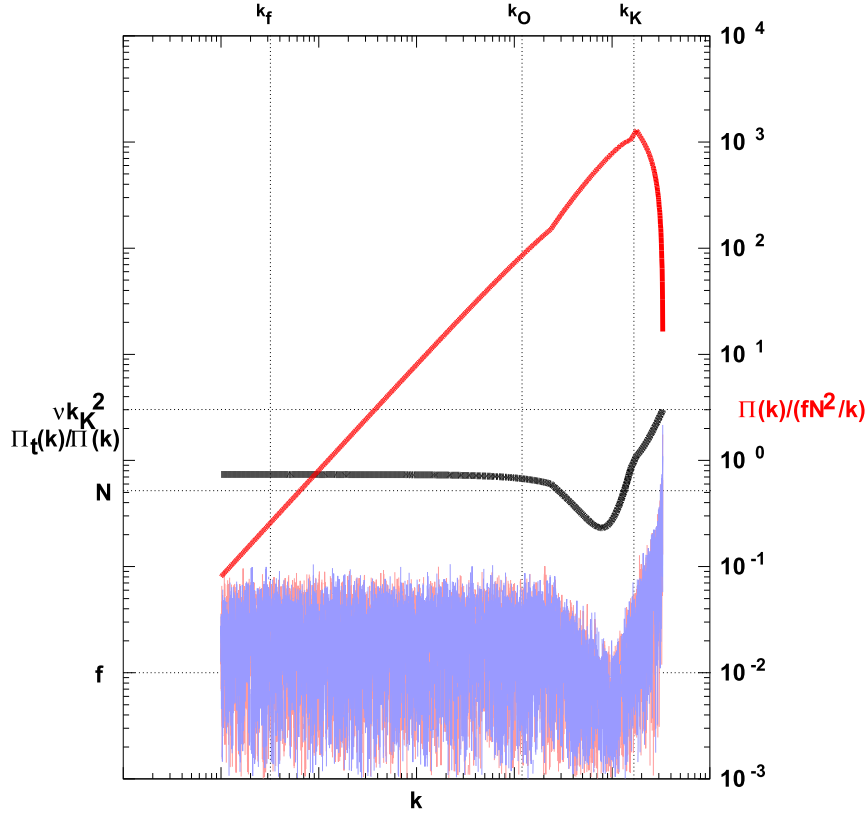


FIG. 7. Convolution spectra for the time rate of change of potential vorticity $\tilde{\Pi}_t(k)$ [(12)] normalized by the maximal $\tilde{\Pi}(k)$ convolution [(13)] (red). Perfect coherence between the vorticity and buoyancy gradient vectors across all wavenumbers yields rates $\sim O(N)$ over the anisotropic stratified turbulence band $\sim k_f < k < k_O$ (black curve). Monte Carlo simulations with random relative orientations between the vectors to simulate isotropic turbulence generates potential vorticity anomalies of both signs (pink and blue) at rates $\sim O(0.1N) \sim O(10f)$ across the anisotropic turbulence band.

where strain component $\chi_z = \int u_z dt$, diapycnal diffusivity $K = \gamma \varepsilon / N^2 = \gamma \nu \text{Re}_b$ and mixing coefficient $\gamma \sim 0.2$ (section 5c). The model spectrum $S[\chi_h](k)$ (Table 4) can be used to evaluate the first term on the rhs of (15) assuming $\chi_z \sim (m/k)\chi_h$ in the anisotropic stratified turbulence band

$$\begin{aligned} \langle \chi_z^2 \rangle|_k &= \int_{k_S}^{k_O} S[\chi_z](k) dk = \int_{k_S}^{k_O} \left(\frac{m^2}{k^2} \right) S[\chi_h](k) dk \\ &= \int_{k_S}^{k_O} \left(\frac{m^2}{k^3} \right) dk = \frac{N^2}{\varepsilon^{2/3}} \int_{k_S}^{k_O} \frac{dk}{k^{7/3}}. \end{aligned} \quad (16)$$

Integrating from the upper-bound k_O toward lower k , horizontal diffusivity K_h increases through the anisotropic stratified turbulence band, behaving like the dimensional scaling $\sim k^{-4/3}$ for $k_f < k_S < k_O$ and reaching $K_h \sim \gamma \varepsilon / f^2 \sim KN^2 / f^2$ at $k_S \sim k_f$. For $K = 0.1 \times 10^{-4} \text{ m}^2 \text{ s}^{-1}$, $N = 5 \times 10^{-3} \text{ rad s}^{-1}$ and $f = 10^{-4} \text{ rad s}^{-1}$, this yields $K_h \sim 0.025 \text{ m}^2 \text{ s}^{-1}$, comparable to that inferred

by Young et al. (1982) for $\langle \chi_z^2 \rangle = \langle u_z^2 \rangle / f^2$ for a GM-level internal-wave field, but over an order of magnitude below $\sim 1\text{--}10\text{-km}$ scale estimates from deliberate dye-release experiments in the ocean (Ledwell et al. 1998; Sundermeyer and Ledwell 2001; Shcherbina et al. 2015). However, turbulence and vertical shears are lognormally distributed and correlated since turbulence is generated by unstable shears. Kunze and Sundermeyer (2015) showed that, for observed intermittencies $e \sim 0.1$, the second (Reynolds) term in (15) dominates. Provided that turbulence persists for $O(f^{-1})$ as argued for in section 5a, isopycnal diffusivity K_h is better approximated as

$$K_h = \langle \delta K \delta \chi_z^2 \rangle \sim e \frac{\langle K \rangle}{e} \frac{\langle \chi_z^2 \rangle}{e} = \frac{\langle K \rangle \langle \chi_z^2 \rangle}{e} \quad (17)$$

(Kunze and Sundermeyer 2015). For intermittency $e \sim 0.1$, (17) yields $K_h \sim O(1) \text{ m}^2 \text{ s}^{-1}$ as observed, lending support for these arguments. This is approximate because diapycnal diffusivities are not bimodal as

$\{0, \langle K \rangle / e\}$, which is assumed in (17), but lognormally distributed. Nevertheless, it demonstrates the effect of turbulent intermittency. Intermittency $e \ll 1$ and $\sim O(f^{-1})$ durations of turbulence imply that shear dispersion by this mechanism will be patchy and only smooth out over time scales of weeks. Other mechanisms such as internal-wave Stokes dispersion and vortical-motion stirring may be more uniform. Similar values have been inferred for subinertial vortical-mode stirring (Polzin and Ferrari 2004; Sundermeyer and Lelong 2005) and intermittent internal-wave-driven shear dispersion (Kunze and Sundermeyer 2015). None of these mechanisms have been ruled out, so the mechanism producing ~ 1 -km-scale isopycnal diffusivities $K_h \sim 1 \text{ m}^2 \text{ s}^{-1}$ remains uncertain.

e. Observational testing

Anisotropic stratified turbulence may be difficult to identify in observations and models. It shares the same frequency band $f < u_h < N$ and “dispersion relation” $Nk/(u_h m) \sim O(1)$ as internal gravity waves. Its frequency spectral level is invariant (Table 4) in contrast to the GM model, and frequency spectra are bluer (more positive) for anisotropic turbulence than the GM model spectra though we caution that Doppler smearing by more energetic larger-scale flows will produce similar effects in measurements that are not fully Lagrangian.

Vertical wavenumber m spectral levels appear to be invariant in the anisotropic stratified turbulence (saturated) band (Figs. 1b, 5; Gargett et al. 1981; Smith et al. 1987) and so are a useful reference point though they yield no information about the cascade rate ε . Vertical wavenumber bandwidth m_O/m_f is predicted to be $(N/f)^{1/2}$, narrower in the abyss and high latitude, and independent of cascade rate ε in contrast to the isotropic turbulence bandwidth $m_K/m_O = k_K/k_O \sim [\varepsilon/(\nu N^2)]^{3/4}$. Testing the bandwidth would require vertical resolution of $\sim O(10^{-2})$ m to span the Ozmidov wavenumber $(N^3/\varepsilon)^{1/2} = (\gamma N/K)^{1/2}$ for typical diapycnal diffusivities $K \sim (0.1\text{--}1) \times 10^{-4} \text{ m}^2 \text{ s}^{-1}$. Sampling more turbulent environments would be less restrictive (Klymak and Moum 2007).

Most of the evidence quoted here comes from horizontal measurements (Figs. 1a, 3a,b). For horizontal shear $u_h = ku$ and horizontal buoyancy gradient $b_h = kb$, the $+1/3$ gradient spectral slope is predicted to extend unbroken above and below the Ozmidov wavenumber k_O , rising and falling with dissipation rate as $\varepsilon^{2/3}$ (Figs. 3a,b). This has thus far only been reported by Klymak and Moum (2007) for horizontal temperature gradients T_h . More horizontal measurements resolving across Ozmidov wavenumber k_O are needed to test that these spectra are not discontinuous in slope or level across k_O . These need to be accompanied by

microscale dissipation rates ε measurements both to estimate k_O and determine whether spectral levels vary as $\varepsilon^{2/3}$. Horizontal shears u_h should exceed f for horizontal wavenumbers $k > k_f = (f^3/\varepsilon)^{1/2} = (f/N)^{3/2} k_O$ with Rossby numbers $\delta_f = u_h/f \sim \varepsilon^{1/3} k^{2/3}$ increasing monotonically with k from $\sim O(1)$ at $\sim k_f$ to $\sim O(N/f)$ at k_O . The predicted horizontal bandwidth $k_O/k_f \sim (N/f)^{3/2}$ should vary from ~ 30 in the abyss to ~ 1000 in the pycnocline, independent of ε . Aspect ratios k/m should vary as $k^{2/3}$ from $\sim f/N$ at $k_f \sim (f^3/\varepsilon)^{1/2}$ to ~ 1 at $k_O \sim (N^3/\varepsilon)^{1/2}$. Both vertical strains ξ_z and gradient Froude numbers $\delta_N = u_z/N$ should be ~ 1 and have -1 spectral slopes over $\sim k_f < k < k_O$. These features might be tested with towed CTD chains and high-frequency ADCP measurements but would require vertical and horizontal resolution of $\sim O(10^{-2})$ m to span typical Ozmidov length scales.

The strongest proof of the model's underlying assumptions would be transfer spectra inferring identical forward energy cascade rates below and above the Ozmidov wavenumber that match the turbulent kinetic energy dissipation rate ε .

f. Numerical testing

The full problem, spanning four to six orders of magnitude in horizontal wavenumber k for midlatitude pycnocline and lower-stratosphere buoyancy frequencies $N \sim 10^{-2} \text{ rad s}^{-1}$ (Figs. 1, 2), is beyond the scope of contemporary numerical modeling, which can span three decades (e.g., Brethouwer et al. 2007; Almalkie and de Bruyn Kops 2012; Bartello and Tobias 2013). This has made simulations attempting to straddle k_f or k_O difficult to interpret due to inadequate bandwidth, and may have prevented clean reproduction of the saturated spectrum in vertical wavenumber m because of the large range of horizontal wavenumbers that contribute to it (Fig. 2; Maffioli 2017). Depending on the focus, this burden might be reduced by choosing abyssal stratifications $N \sim 10^{-3} \text{ rad s}^{-1}$ to reduce k_O/k_f or a lower Re_b to reduce k_K/k_O . Reduced bandwidths would make it more difficult to unambiguously identify spectral slopes, for example, the isotropic turbulence band is expected to vanish for $\text{Re}_b < O(100)$ (Gargett et al. 1984) and $m_O/m_f < 3$ for $N/f < 10$. Most simulations of anisotropic stratified turbulence have focused on $u_h < N$ (Billant and Chomaz 2001; Riley and de Bruyn Kops 2003; Waite and Bartello 2004; Lindborg 2006; Brethouwer et al. 2007), have been irrotational, used anisotropic grids, and forced with potential vorticity anomalies. These preconditions are suitable for studying the middle of the stratified turbulence band $k_f \ll k \ll k_O$ (Fig. 6) but not (i) anisotropic generation by internal-wave instabilities at $k \ll k_O$ or (ii) the transition to isotropic turbulence at k_O .

These two subproblems are of special interest because they involve a change in dynamics and behavior. The first would establish that an anisotropic forward turbulent cascade can be triggered by anisotropic instability of finescale $\sim f/N$ aspect ratio near-inertial wave packets at $k \ll k_O$ where rotation and horizontal shears are important. To the author's knowledge, this problem has not been examined theoretically or numerically. Numerically, it could be treated with anisotropic grids $\sim O(f/N)$ at moderate buoyancy Reynolds number, allowing the resulting anisotropic turbulence to dissipate via a subgrid-scale damping parameterization like hyperviscosity at $k < k_O$ before becoming isotropic. Marginally unstable ($\delta_N \sim \delta_f \sim 1$) wave packets could be forced into instability by subjecting them to a wave-capture scenario (Bühler and McIntyre 2005) where both vertical and horizontal wavenumbers increase, forcing group velocities to shrink and shears to amplify. If source instability and dissipative scales are sufficiently separated, these simulations could identify when during the cascade process potential vorticity arises at wavenumbers well below those associated with dissipation. Waite and Bartello (2006a) attempted to investigate internal-wave generation of anisotropic stratified turbulence but reported inconclusive results.

The second problem would study the transition from anisotropic stratified turbulence at $k < k_O$ to isotropic turbulence and density overturning at $k \sim k_O$ where $u_h \sim N$. This would require an isotropic grid and buoyancy Reynolds numbers sufficiently high to ensure isotropy at the transition (e.g., $Re_b > 200$; Gargett et al. 1984). The full inertial isotropic cascade might not need to be resolved if dissipation could be handled with hyperviscosity (e.g., Winters and D'Asaro 1994). Such simulations would be initialized with $k < k_O$ anisotropic stratified turbulence based on the simulations described in the previous paragraph, consistent with the desired buoyancy Reynolds number and lowest resolved wavenumber, then allowed to evolve.

Both of these subproblems have been studied but proven challenging to implement and hard to interpret because of aphysical forcing at low wavenumber and uncertain influences on the intermediate wavenumber domain by both the low-wavenumber forcing and high-wavenumber dissipation.

Another question is whether numerical simulations could produce a forward energy cascade in the absence of potential vorticity forcing. Most of the model simulations have been initialized with barotropic vortices that break down into lower aspect ratio layers via the zigzag instability (Billant and Chomaz 2000), or forced spectrally at lower wavenumbers then allowed to relax to stratified turbulence (Lindborg 2006). Neither of

these forcings excludes potential vorticity. It would be illuminating to contrast the properties of numerically simulated anisotropic stratified turbulence and its cascade with and without potential vorticity forcing.

6. Concluding remarks

A new interpretation is offered for ocean and atmosphere horizontal and vertical wavenumber spectra in the decade or so below the Ozmidov wavenumber $k_O = m_O = (N^3/\epsilon)^{1/2}$ (Fig. 1), that is, on scales between those attributed to internal waves [$m < m_c \sim N(f/\epsilon)^{1/2}$] and isotropic turbulence ($m > m_O$) (Fig. 1). Based on the forward energy cascade reported in the atmosphere (Lindborg and Cho 2000), ocean (Poje et al. 2017), and numerical simulations (Waite and Bartello 2004; Lindborg 2006; Brethouwer et al. 2007), this band is identified as anisotropic stratified turbulence following Riley and Lindborg (2008). A spectral model constructed from dimensional scaling (section 2; Table 4; Figs. 3–5) reproduces the observations summarized in Fig. 1. Anisotropic stratified turbulence does not occupy the full parameter space of Rossby number, gradient Froude number, and energy ratio R_E but is constrained to have $1 < \delta_f < N/f$ (Lindborg 2006), $\delta_N \sim O(1)$ (Billant and Chomaz 2001) and $R_E \sim 1$. It shares a “dispersion relation” with internal waves, that is, $m/k \sim N/u_h$, with straining frequency u_h replacing the intrinsic wave frequency and lying in the internal-wave band $f < u_h < N$ (section 3c; Fig. 4).

The most novel implication of this interpretation is that small-scale geophysical turbulence is made up of both anisotropic stratified and isotropic turbulence such that the anisotropic turbulent energy cascade feeds smoothly into the isotropic turbulent cascade as it crosses the Ozmidov wavenumber (section 5a). This further implies that isotropic turbulence in the stratified ocean need not be directly generated by internal-wave breaking as commonly assumed. Rather, anisotropic instability of finescale near-inertial wave packets can feed energy into anisotropic stratified turbulence at horizontal wavenumbers $k_S \ll k_O$, which then cascades downscale through the isotropic turbulence band to dissipation (section 5a; Fig. 6).

The interpretation of submesoscale and finescale data presented here is by no means certain, based on multiple unique measurements that have often been interpreted differently. While linear internal gravity waves have been ruled out (Müller et al. 1988; Polzin et al. 2003) and linearity in general seems unlikely on the finescale where $u_z \sim N$ and $u_h > f$, either nonlinear internal waves or a variant of the turbulent forward cascade in horizontal wavenumber proposed here remain possible. Many of the assumptions and conclusions require rigorous testing

including that (i) aspect ratio $\sim f/N$ finescale near-inertial wave packets in the ocean become anisotropically unstable at horizontal wavenumbers $k \ll k_O$ to produce anisotropic stratified turbulence (Fig. 6), (ii) variance at wavenumbers $\sim k_f < k < k_O$ has invariant energy ratio $KE/APE \sim O(1)$ at all horizontal wavenumbers k and cascades energy forward uniformly with k (section 2), (iii) the transition from anisotropic to isotropic turbulence occurs smoothly across the Ozmidov wavenumber k_O with no change in spectral slope or level for u_h or b_h/N^2 (Figs. 3, 4), and (iv) the cascade rate below and above the Ozmidov wavenumber is identically the microscale dissipation rate ε . It is hoped that the work presented here will provide a framework to help unravel the dynamics of finescale motions in the decade or so below the Ozmidov wavenumber $k_O = (N^3/\varepsilon)^{1/2}$ in the ocean, atmosphere, and other stratified fluids.

Acknowledgments. Ren-Chieh Lien is thanked for his careful reading that identified several inconsistencies in an earlier draft. This work also benefited from the input of Pascale Lelong, Eric D'Asaro, Jim Riley, Jeffrey Early, Richard Scott, Kraig Winters, Cimarron Wortham, and two anonymous reviewers. It was made possible by NSF Grants OCE-1536747 and OCE-1734222.

REFERENCES

- Almalkie, S., and S. M. de Bruyn Kops, 2012: Kinematic energy dynamics in forced, homogeneous and axisymmetric stably stratified flows. *J. Turbul.*, **13**, N29, <https://doi.org/10.1080/14685248.2012.702909>.
- Barry, M. E., G. N. Ivey, K. B. Winters, and J. Imberger, 2001: Measurements of diapycnal diffusivities in stratified fluids. *J. Fluid Mech.*, **442**, 267–291, <https://doi.org/10.1017/S0022112001005080>.
- Bartello, P., and S. M. Tobias, 2013: Sensitivity of stratified turbulence to the buoyancy Reynolds number. *J. Fluid Mech.*, **725**, 1–22, <https://doi.org/10.1017/jfm.2013.170>.
- Batchelor, G. K., 1953: *The Theory of Homogeneous Turbulence*. Cambridge University Press, 201 pp.
- , 1959: Small-scale variation of convected quantities like temperature in turbulent fluid. *J. Fluid Mech.*, **5**, 113–139, <https://doi.org/10.1017/S002211205900009X>.
- Billant, P., and J.-M. Chomaz, 2000: Experimental evidence for a new instability of a vertical columnar vortex pair in a strongly stratified fluid. *J. Fluid Mech.*, **418**, 167–188, <https://doi.org/10.1017/S0022112000001154>.
- , and —, 2001: Self-similarity of strongly stratified inviscid flows. *Phys. Fluids*, **13**, 1645–1651, <https://doi.org/10.1063/1.1369125>.
- Bluteau, C. E., N. L. Jones, and G. N. Ivey, 2013: Turbulent mixing efficiency at an energetic ocean site. *J. Geophys. Res. Oceans*, **118**, 4662–4672, <https://doi.org/10.1002/jgrc.20292>.
- Brethouwer, G., P. Billant, E. Lindborg, and J.-M. Chomaz, 2007: Scaling analysis and simulation of sternly stratified turbulent flows. *J. Fluid Mech.*, **585**, 343–368, <https://doi.org/10.1017/S0022112007006854>.
- Briscoe, M. G., 1977: On current finestructure and moored current meter measurements of internal waves. *Deep-Sea Res.*, **24**, 1121–1131, [https://doi.org/10.1016/0146-6291\(77\)90516-1](https://doi.org/10.1016/0146-6291(77)90516-1).
- Bühler, O., and M. E. McIntyre, 2005: Wave capture and wave-vortex duality. *J. Fluid Mech.*, **534**, 67–95, <https://doi.org/10.1017/S0022112005004374>.
- , J. Callies, and R. Ferrari, 2014: Wave-vortex decomposition of one-dimensional ship-track data. *J. Fluid Mech.*, **756**, 1007–1026, <https://doi.org/10.1017/jfm.2014.488>.
- Callies, J., R. Ferrari, and O. Bühler, 2014: Transition from geostrophic turbulence to inertia-gravity waves in the atmospheric energy spectrum. *Proc. Natl. Acad. Sci. USA*, **111**, 17 033–17 038, <https://doi.org/10.1073/pnas.1410772111>.
- , —, J. M. Klymak, and J. Gula, 2015: Seasonality in submesoscale turbulence. *Nat. Commun.*, **6**, 6862, <https://doi.org/10.1038/ncomms7862>.
- , O. Bühler, and R. Ferrari, 2016: The dynamics of mesoscale winds in the upper troposphere and lower stratosphere. *J. Atmos. Sci.*, **73**, 4853–4872, <https://doi.org/10.1175/JAS-D-16-0108.1>.
- Charney, J. G., 1971: Geostrophic turbulence. *J. Atmos. Sci.*, **28**, 1087–1095, [https://doi.org/10.1175/1520-0469\(1971\)028<1087:GT>2.0.CO;2](https://doi.org/10.1175/1520-0469(1971)028<1087:GT>2.0.CO;2).
- D'Asaro, E. A., and H. Perkins, 1984: The near-inertial internal wave spectrum in the late summer Sargasso Sea. *J. Phys. Oceanogr.*, **14**, 781–794, [https://doi.org/10.1175/1520-0485\(1984\)014<0781:WFIWIT>2.0.CO;2](https://doi.org/10.1175/1520-0485(1984)014<0781:WFIWIT>2.0.CO;2).
- , and R.-C. Lien, 2000: The wave-turbulence transition for stratified flows. *J. Phys. Oceanogr.*, **30**, 1669–1678, [https://doi.org/10.1175/1520-0485\(2000\)030<1669:TWTFS>2.0.CO;2](https://doi.org/10.1175/1520-0485(2000)030<1669:TWTFS>2.0.CO;2).
- Davis, K. A., and S. G. Monismith, 2011: The modification of bottom-boundary-layer turbulence and mixing by internal waves shoaling on a barrier reef. *J. Phys. Oceanogr.*, **41**, 2223–2241, <https://doi.org/10.1175/2011JPO4344.1>.
- Desaubies, Y. J. F., 1975: A linear theory of internal wave spectra and coherences near the Vaisala frequency. *J. Geophys. Res.*, **80**, 895–899, <https://doi.org/10.1029/JC080i006p00895>.
- Dewan, E. M., 1979: Stratospheric spectra resembling turbulence. *Science*, **204**, 832–835, <https://doi.org/10.1126/science.204.4395.832>.
- , 1997: Saturated-cascade similitude theory of gravity wave spectra. *J. Geophys. Res.*, **102**, 29 799–29 817, <https://doi.org/10.1029/97JD02151>.
- , and R. E. Good, 1986: Saturation and the universal spectrum for vertical profiles of horizontal scalar winds in the atmosphere. *J. Geophys. Res.*, **91**, 2742–2748, <https://doi.org/10.1029/JD091iD02p02742>.
- Duda, T. F., and C. S. Cox, 1989: Vertical wavenumber spectra of velocity and shear at small internal-wave scales. *J. Geophys. Res.*, **94**, 939–950, <https://doi.org/10.1029/JC094iC01p00939>.
- Eckermann, S. D., 1999: Isentropic advection by gravity waves: Quasi-universal M^{-3} vertical wavenumber spectra at the onset of instability. *Geophys. Res. Lett.*, **26**, 201–204, <https://doi.org/10.1029/1998GL900283>.
- Ertel, H., 1942: Ein neuer hydrodynamischer wirbelsatz. *Meteor. Z.*, **59**, 277–281.
- Ewart, T. E., 1976: Observations from straightline isobaric runs of SPURV. *Proc. IAPSO/IAPMAP PSH*, Edinburgh, United Kingdom, Joint Oceanographic Assembly, 1–18.
- Falder, M., N. J. White, and C. P. Caulfield, 2016: Seismic imaging of rapid onset stratified turbulence in the South Atlantic Ocean. *J. Phys. Oceanogr.*, **46**, 1023–1044, <https://doi.org/10.1175/JPO-D-15-0140.1>.
- Fortin, W. F. J., W. S. Holbrook, and R. W. Schmitt, 2016: Mapping turbulent diffusivity associated with oceanic internal lee waves

- offshore Costa Rica. *Ocean Sci.*, **12**, 601–612, <https://doi.org/10.5194/os-12-601-2016>.
- Fritts, D. C., 1984: Gravity wave saturation in the middle atmosphere: A review of theory and observations. *Rev. Geophys.*, **22**, 275–308, <https://doi.org/10.1029/RG022i003p00275>.
- , T. Tsuda, S. Kato, T. Sato, and S. Fukao, 1988: Observational evidence of a saturated gravity wave spectrum in the troposphere and lower stratosphere. *J. Atmos. Sci.*, **45**, 1741–1759, [https://doi.org/10.1175/1520-0469\(1988\)045<1741:OEOASG>2.0.CO;2](https://doi.org/10.1175/1520-0469(1988)045<1741:OEOASG>2.0.CO;2).
- Gage, K. S., 1979: Evidence for a $k^{-5/3}$ law inertial range in mesoscale two-dimensional turbulence. *J. Atmos. Sci.*, **36**, 1950–1954, [https://doi.org/10.1175/1520-0469\(1979\)036<1950:EFALIR>2.0.CO;2](https://doi.org/10.1175/1520-0469(1979)036<1950:EFALIR>2.0.CO;2).
- Gargett, A. E., P. J. Hendricks, T. B. Sanford, T. R. Osborn, and A. J. Williams, 1981: A composite spectrum of vertical shear in the ocean. *J. Phys. Oceanogr.*, **11**, 1258–1271, [https://doi.org/10.1175/1520-0485\(1981\)011<1258:ACSOVS>2.0.CO;2](https://doi.org/10.1175/1520-0485(1981)011<1258:ACSOVS>2.0.CO;2).
- , T. R. Osborn, and P. W. Nasmyth, 1984: Local isotropy and the decay of turbulence in a stratified fluid. *J. Fluid Mech.*, **144**, 231–280, <https://doi.org/10.1017/S0022112084001592>.
- Garrett, C., and W. Munk, 1979: Internal waves in the ocean. *Annu. Rev. Fluid Mech.*, **11**, 339–369, <https://doi.org/10.1146/annurev.fl.11.010179.002011>.
- Gregg, M. C., 1989: Scaling turbulent dissipation in the thermocline. *J. Geophys. Res.*, **94**, 9686–9698, <https://doi.org/10.1029/JC094iC07p09686>.
- , and E. Kunze, 1991: Internal wave shear and strain in Santa Monica Basin. *J. Geophys. Res.*, **96**, 16 709–16 719, <https://doi.org/10.1029/91JC01385>.
- , E. A. D'Asaro, T. J. Shay, and N. Larson, 1986: Observations of persistent mixing and near-inertial internal waves. *J. Phys. Oceanogr.*, **16**, 856–885, [https://doi.org/10.1175/1520-0485\(1986\)016<0856:OOPMAN>2.0.CO;2](https://doi.org/10.1175/1520-0485(1986)016<0856:OOPMAN>2.0.CO;2).
- , D. P. Winkel, and T. B. Sanford, 1993: Varieties of fully resolved spectra of vertical shear. *J. Phys. Oceanogr.*, **23**, 124–141, [https://doi.org/10.1175/1520-0485\(1993\)023<0124:VOFRSO>2.0.CO;2](https://doi.org/10.1175/1520-0485(1993)023<0124:VOFRSO>2.0.CO;2).
- , T. B. Sanford, and D. P. Winkel, 2003: Reduced mixing from the breaking of internal waves in equatorial waters. *Nature*, **422**, 513–515, <https://doi.org/10.1038/nature01507>.
- , E. A. D'Asaro, J. J. Riley, and E. Kunze, 2018: Mixing efficiency in the ocean. *Ann. Rev. Ocean Sci.*, **10**, 443–473, <https://doi.org/10.1146/annurev-marine-121916-063643>.
- Hebert, D., and J. N. Moum, 1994: Decay of a near-inertial wave. *J. Phys. Oceanogr.*, **24**, 2334–2351, [https://doi.org/10.1175/1520-0485\(1994\)024<2334:DOANIW>2.0.CO;2](https://doi.org/10.1175/1520-0485(1994)024<2334:DOANIW>2.0.CO;2).
- Heney, F. S., J. Wright, and S. M. Flatté, 1986: Energy and action flow through the internal-wave field. *J. Geophys. Res.*, **91**, 8487–8495, <https://doi.org/10.1029/JC091iC07p08487>.
- Hines, C. O., 1993: The saturation of gravity waves in the middle atmosphere. Part IV: Cutoff of the incident wavenumber spectrum. *J. Atmos. Sci.*, **50**, 3045–3060, [https://doi.org/10.1175/1520-0469\(1993\)050<3045:TSOGWI>2.0.CO;2](https://doi.org/10.1175/1520-0469(1993)050<3045:TSOGWI>2.0.CO;2).
- Holbrook, W. S., and I. Fer, 2005: Ocean internal wave spectra inferred from seismic reflection transits. *Geophys. Res. Lett.*, **32**, L15604, <https://doi.org/10.1029/2005GL023733>.
- , —, R. W. Schmitt, D. Lizzaralde, J. M. Klymak, L. C. Helfrich, and R. Kubichek, 2013: Estimating oceanic turbulence dissipation from seismic images. *J. Atmos. Oceanic Technol.*, **30**, 1767–1788, <https://doi.org/10.1175/JTECH-D-12-00140.1>.
- Ijichi, T., and T. Hibiya, 2018: Observed variations in turbulent mixing efficiency in the deep ocean. *J. Phys. Oceanogr.*, **48**, 1815–1830, <https://doi.org/10.1175/JPO-D-17-0275.1>.
- Itsweire, E. C., T. R. Osborn, and T. P. Stanton, 1989: Horizontal distribution and characteristics of shear layers in the seasonal thermocline. *J. Phys. Oceanogr.*, **19**, 301–320, [https://doi.org/10.1175/1520-0485\(1989\)019<0301:HDACOS>2.0.CO;2](https://doi.org/10.1175/1520-0485(1989)019<0301:HDACOS>2.0.CO;2).
- Klymak, J. M., and J. N. Moum, 2007: Oceanic isopycnal slope spectra. Part II: Turbulence. *J. Phys. Oceanogr.*, **37**, 1232–1245, <https://doi.org/10.1175/JPO3074.1>.
- Kolmogorov, A., 1941: The local structure of turbulence in incompressible viscous fluids for very large Reynolds number. *Dokl. Akad. Nauk SSSR*, **30**, 199–303.
- Kunze, E., 2014: The relation between unstable shear layer thicknesses and turbulence lengthscales. *J. Mar. Res.*, **72**, 95–104, <https://doi.org/10.1357/002224014813758977>.
- , and M. A. Sundermeyer, 2015: The role of intermittency in internal-wave shear dispersion. *J. Phys. Oceanogr.*, **45**, 2979–2990, <https://doi.org/10.1175/JPO-D-14-0134.1>.
- , A. J. Williams III, and M. G. Briscoe, 1990: Observations of shear and vertical stability from a neutrally buoyant float. *J. Geophys. Res.*, **95**, 18 127–18 142, <https://doi.org/10.1029/JC095iC10p18127>.
- , R. W. Schmitt, and J. M. Toole, 1995: The energy balance in a warm-core ring's near-inertial critical layer. *J. Phys. Oceanogr.*, **25**, 942–957, [https://doi.org/10.1175/1520-0485\(1995\)025<0942:TEBIAW>2.0.CO;2](https://doi.org/10.1175/1520-0485(1995)025<0942:TEBIAW>2.0.CO;2).
- , J. M. Klymak, R.-C. Lien, R. Ferrari, C. M. Lee, M. A. Sundermeyer, and L. Goodman, 2015: Submesoscale water-mass spectra in the Sargasso Sea. *J. Phys. Oceanogr.*, **45**, 1325–1338, <https://doi.org/10.1175/JPO-D-14-0108.1>.
- Laval, J.-P., J. C. McWilliams, and B. Dubrulle, 2003: Forced stratified turbulence: Successive transitions with Reynolds number. *Phys. Rev. E*, **68**, 036308, <https://doi.org/10.1103/PhysRevE.68.036308>.
- Ledwell, J. R., A. J. Watson, and C. S. Law, 1998: Mixing on a tracer in the pycnocline. *J. Geophys. Res.*, **103**, 21 499–21 529, <https://doi.org/10.1029/98JC01738>.
- Lelong, M.-P., 1989: Weakly nonlinear internal wave/vortical mode interactions in stably-stratified flows. Ph.D. thesis, University of Washington, 108 pp.
- Lighthill, J., 1978: *Waves in Fluids*. Cambridge University Press, 317–337.
- Lilly, D. K., 1983: Stratified turbulence and the mesoscale variability of the atmosphere. *J. Atmos. Sci.*, **40**, 749–761, [https://doi.org/10.1175/1520-0469\(1983\)040<0749:STATMV>2.0.CO;2](https://doi.org/10.1175/1520-0469(1983)040<0749:STATMV>2.0.CO;2).
- Lindborg, E., 2005: The effect of rotation on the mesoscale energy cascade in the free atmosphere. *Geophys. Res. Lett.*, **32**, L01809, <https://doi.org/10.1029/2004GL021319>.
- , 2006: The energy cascade in a strongly stratified fluid. *J. Fluid Mech.*, **550**, 207–241, <https://doi.org/10.1017/S0022112005008128>.
- , and J. Y. N. Cho, 2000: Determining the cascade of passive scalar variance in the lower stratosphere. *Phys. Rev. Lett.*, **85**, 5663–5666, <https://doi.org/10.1103/PhysRevLett.85.5663>.
- Lozovatsky, I. D., and H. J. S. Fernando, 2012: Mixing efficiency in natural flows. *Philos. Trans. Roy. Soc.*, **371A**, 20120213, <https://doi.org/10.1098/rsta.2012.0213>.
- Müller, P., D. J. Olbers, and J. Willebrand, 1978: The IWEX spectrum. *J. Geophys. Res.*, **83**, 479–500, <https://doi.org/10.1029/JC083iC01p00479>.
- , G. Holloway, F. Heney, and N. Pomphrey, 1986: Nonlinear interactions among internal gravity waves. *Rev. Geophys.*, **24**, 493–536, <https://doi.org/10.1029/RG024i003p00493>.
- , R.-C. Lien, and R. Williams, 1988: Estimates of potential vorticity at small scales in the ocean. *J. Phys. Oceanogr.*, **18**,

- 401–416, [https://doi.org/10.1175/1520-0485\(1988\)018<0401:EOPVAS>2.0.CO;2](https://doi.org/10.1175/1520-0485(1988)018<0401:EOPVAS>2.0.CO;2).
- Maffioli, A., 2017: Vertical spectra of stratified turbulence at large horizontal scales. *Phys. Rev. Fluids*, **2**, 104802, <https://doi.org/10.1103/PhysRevFluids.2.104802>.
- Marmorino, G. O., 1987: Observations of small-scale mixing processes in the seasonal thermocline. Part II: Wave breaking. *J. Phys. Oceanogr.*, **17**, 1348–1355, [https://doi.org/10.1175/1520-0485\(1987\)017<1348:OOSMP>2.0.CO;2](https://doi.org/10.1175/1520-0485(1987)017<1348:OOSMP>2.0.CO;2).
- , and C. L. Trump, 1991: “Turbulent mixing” induced by upgoing near-inertial waves in the seasonal thermocline of the Norwegian Sea. *J. Geophys. Res.*, **96**, 7137–7143, <https://doi.org/10.1029/91JC00084>.
- , L. J. Rosenblum, and C. L. Trump, 1987: Finescale temperature variability: The influence of near-inertial waves. *J. Geophys. Res.*, **92**, 13 049–13 062, <https://doi.org/10.1029/JC092iC12p13049>.
- Mashayek, A., C. P. Caulfield, and W. R. Peltier, 2017: Role of overturns in optical mixing in stratified mixing layers. *J. Fluid Mech.*, **826**, 522–552, <https://doi.org/10.1017/jfm.2017.374>.
- McComas, H. C., and P. Müller, 1981: The dynamic balance of internal waves. *J. Phys. Oceanogr.*, **11**, 970–986, [https://doi.org/10.1175/1520-0485\(1981\)011<0970:TDBOIW>2.0.CO;2](https://doi.org/10.1175/1520-0485(1981)011<0970:TDBOIW>2.0.CO;2).
- Miles, J. W., 1961: On the stability of heterogeneous shear flows. *J. Fluid Mech.*, **10**, 496–512, <https://doi.org/10.1017/S0022112061000305>.
- Moum, J. N., 2015: Ocean speed and turbulence measurements using pitot-static tubes on moorings. *J. Atmos. Oceanic Technol.*, **32**, 1400–1413, <https://doi.org/10.1175/JTECH-D-14-00158.1>.
- Nastrom, G. D., and K. S. Gage, 1985: A climatology of atmospheric wavenumber spectra of wind and temperature observed by commercial aircraft. *J. Atmos. Sci.*, **42**, 950–960, [https://doi.org/10.1175/1520-0469\(1985\)042<0950:ACOWS>2.0.CO;2](https://doi.org/10.1175/1520-0469(1985)042<0950:ACOWS>2.0.CO;2).
- Oakey, N. S., 1982: Determination of the rate of dissipation of turbulent energy from simultaneous temperature and velocity shear microstructure measurements. *J. Phys. Oceanogr.*, **12**, 256–271, [https://doi.org/10.1175/1520-0485\(1982\)012<0256:DOTROD>2.0.CO;2](https://doi.org/10.1175/1520-0485(1982)012<0256:DOTROD>2.0.CO;2).
- Ozmidov, R. V., 1965: On the turbulent exchange in a stably stratified ocean. *Izv. Acad. Sci. USSR, Atmos. Oceanic Phys.*, **1**, 853–860.
- Pinkel, R., 2014: Vortical and internal wave shear and strain. *J. Phys. Oceanogr.*, **44**, 2070–2092, <https://doi.org/10.1175/JPO-D-13-090.1>.
- Poje, A. C., T. M. Özgökmen, D. J. Bogucki, and A. D. Kirwan Jr., 2017: Evidence of a forward energy cascade and Kolmogorov self-similarity in submesoscale ocean surface-drifter observations. *Phys. Fluids*, **29**, 020701, <https://doi.org/10.1063/1.4974331>.
- Polzin, K., 1996: Statistics of Richardson number: Mixing models and finestructure. *J. Phys. Oceanogr.*, **26**, 1409–1425, [https://doi.org/10.1175/1520-0485\(1996\)026<1409:SOTRNM>2.0.CO;2](https://doi.org/10.1175/1520-0485(1996)026<1409:SOTRNM>2.0.CO;2).
- , and R. Ferrari, 2004: Isopycnal dispersion in NATRE. *J. Phys. Oceanogr.*, **34**, 247–257, [https://doi.org/10.1175/1520-0485\(2004\)034<0247:IDIN>2.0.CO;2](https://doi.org/10.1175/1520-0485(2004)034<0247:IDIN>2.0.CO;2).
- , J. M. Toole, and R. W. Schmitt, 1995: Finescale parameterization of turbulent dissipation. *J. Phys. Oceanogr.*, **25**, 306–328, [https://doi.org/10.1175/1520-0485\(1995\)025<0306:FPOTD>2.0.CO;2](https://doi.org/10.1175/1520-0485(1995)025<0306:FPOTD>2.0.CO;2).
- , E. Kunze, J. M. Toole, and R. W. Schmitt, 2003: The partition of finescale energy into internal waves and geostrophic motions. *J. Phys. Oceanogr.*, **33**, 234–248, [https://doi.org/10.1175/1520-0485\(2003\)033<0234:TPOFEI>2.0.CO;2](https://doi.org/10.1175/1520-0485(2003)033<0234:TPOFEI>2.0.CO;2).
- Riley, J. J., and S. M. deBruynKops, 2003: Dynamics of turbulence strongly influenced by buoyancy. *Phys. Fluids*, **15**, 2047, <https://doi.org/10.1063/1.1578077>.
- , and E. Lindborg, 2008: Stratified turbulence: A possible interpretation of some geophysical turbulence measurements. *J. Atmos. Sci.*, **65**, 2416–2424, <https://doi.org/10.1175/2007JAS2455.1>.
- , R. W. Metcalfe, and M. A. Weisman, 1981: Direct numerical simulations of homogeneous turbulence in density-stratified fluids. *Proc. AIP Conf. on Nonlinear Properties of Internal Waves*, Houston, TX, American Institute of Physics, 79–112.
- Rosenblum, L. J., and G. O. Marmorino, 1990: Statistics of mixing patches observed in the Sargasso Sea. *J. Geophys. Res.*, **95**, 5349–5357, <https://doi.org/10.1029/JC095iC04p05349>.
- Shcherbina, A. Y., and Coauthors, 2015: The LatMix summer campaign: Submesoscale stirring in the upper ocean. *Bull. Amer. Meteor. Soc.*, **96**, 1257–1279, <https://doi.org/10.1175/BAMS-D-14-00015.1>.
- Sheen, K. L., N. J. White, and R. W. Hobbs, 2009: Estimating mixing rates from seismic images of oceanic structure. *Geophys. Res. Lett.*, **36**, L00D04, <https://doi.org/10.1029/2009GL040106>.
- Shih, L. H., J. R. Koseff, G. N. Ivey, and J. H. Ferziger, 2005: Parameterization of turbulent fluxes and scales using homogeneous sheared stably stratified turbulence simulations. *J. Fluid Mech.*, **525**, 193–214, <https://doi.org/10.1017/S0022112004002587>.
- Smith, S. A., D. C. Fritts, and T. E. Vanzandt, 1987: Evidence for a saturated spectrum of atmospheric gravity waves. *J. Atmos. Sci.*, **44**, 1404–1410, [https://doi.org/10.1175/1520-0469\(1987\)044<1404:EFASSO>2.0.CO;2](https://doi.org/10.1175/1520-0469(1987)044<1404:EFASSO>2.0.CO;2).
- Smyth, W. D., J. N. Moum, and D. R. Caldwell, 2001: The efficiency of turbulent patches: Inferences from direct simulations and microstructure observations. *J. Phys. Oceanogr.*, **31**, 1969–1992, [https://doi.org/10.1175/1520-0485\(2001\)031<1969:TEOMIT>2.0.CO;2](https://doi.org/10.1175/1520-0485(2001)031<1969:TEOMIT>2.0.CO;2).
- St. Laurent, L. S., and R. W. Schmitt, 1999: The contributions of salt fingers to vertical mixing in the North Atlantic Tracer Release Experiment. *J. Phys. Oceanogr.*, **29**, 1404–1424, [https://doi.org/10.1175/1520-0485\(1999\)029<1404:TCOSFT>2.0.CO;2](https://doi.org/10.1175/1520-0485(1999)029<1404:TCOSFT>2.0.CO;2).
- Sundermeyer, M. A., and J. R. Ledwell, 2001: Lateral dispersion over the continental shelf: Analysis of dye-release experiments. *J. Geophys. Res.*, **106**, 9603–9621, <https://doi.org/10.1029/2000JC900138>.
- , and M.-P. Lelong, 2005: Numerical simulations of lateral dispersion by the relaxation of diapycnal mixing events. *J. Phys. Oceanogr.*, **35**, 2368–2386, <https://doi.org/10.1175/JPO2834.1>.
- Taylor, G. I., 1935: Statistical theory of turbulence. *Proc. Roy. Soc. London*, **151A**, 421–478, <https://doi.org/10.1098/rspa.1935.0158>.
- Tennekes, H., and J. L. Lumley, 1972: *A First Course in Turbulence*. MIT Press, 300 pp.
- Thorpe, S. A., 1973: Experiments on instability and turbulence in a stratified shear flow. *J. Fluid Mech.*, **61**, 731–751, <https://doi.org/10.1017/S0022112073000911>.
- , 1978: On the shape and breaking of finite-amplitude internal gravity waves in a shear flow. *J. Fluid Mech.*, **85**, 7–32, <https://doi.org/10.1017/S0022112078000518>.

- , 2005: *The Turbulent Ocean*. Cambridge University Press, 439 pp.
- Waite, M. L., and P. Bartello, 2004: Stratified turbulence dominated by vertical motion. *J. Fluid Mech.*, **517**, 281–308, <https://doi.org/10.1017/S0022112004000977>.
- , and ———, 2006a: Stratified turbulence generated by internal gravity waves. *J. Fluid Mech.*, **546**, 313–339, <https://doi.org/10.1017/S0022112005007111>.
- , and ———, 2006b: The transition from geostrophic to stratified turbulence. *J. Fluid Mech.*, **568**, 89–108, <https://doi.org/10.1017/S0022112006002060>.
- Whalen, C. B., J. A. MacKinnon, L. D. Talley, and A. F. Waterhouse, 2015: Estimating the main diapycnal mixing using a finescale strain parameterization. *J. Phys. Oceanogr.*, **45**, 1174–1188, <https://doi.org/10.1175/JPO-D-14-0167.1>.
- Winters, K. B., and E. A. D’Asaro, 1994: Three-dimensional wave instability near a critical level. *J. Fluid Mech.*, **272**, 255–284, <https://doi.org/10.1017/S0022112094004465>.
- Young, W. R., P. B. Rhines, and C. J. R. Garrett, 1982: Shear-flow dispersion, internal waves and horizontal mixing in the ocean. *J. Phys. Oceanogr.*, **12**, 515–527, [https://doi.org/10.1175/1520-0485\(1982\)012<0515:SFDIWA>2.0.CO;2](https://doi.org/10.1175/1520-0485(1982)012<0515:SFDIWA>2.0.CO;2).